

DYNAMIC ACTIVITY AND CRUSHED ICE BEHAVIOR IN  
MEDIUM-SCALE ICE-STRUCTURE INTERACTIONS

CENTRE FOR NEWFOUNDLAND STUDIES

**TOTAL OF 10 PAGES ONLY  
MAY BE XEROXED**

(Without Author's Permission)

KURT PATRICK KENNEDY, B.Eng.







# **Dynamic Activity and Crushed Ice Behavior in Medium-Scale Ice-Structure Interactions**

by

© Kurt Patrick Kennedy, B.Eng.

A thesis submitted to the School of Graduate Studies  
in partial fulfillment of the requirements for the degree of  
Master of Engineering

Faculty of Engineering and Applied Science  
Memorial University of Newfoundland  
October, 1990

St. John's

Newfoundland

Canada



National Library  
of Canada

Bibliothèque nationale  
du Canada

Canadian Theses Service    Service des thèses canadiennes

Ottawa, Canada  
K1A 0N4

The author has granted an irrevocable non-exclusive licence allowing the National Library of Canada to reproduce, loan, distribute or sell copies of his/her thesis by any means and in any form or format, making this thesis available to interested persons.

The author retains ownership of the copyright in his/her thesis. Neither the thesis nor substantial extracts from it may be printed or otherwise reproduced without his/her permission.

L'auteur a accordé une licence irrévocable et non exclusive permettant à la Bibliothèque nationale du Canada de reproduire, prêter, distribuer ou vendre des copies de sa thèse de quelque manière et sous quelque forme que ce soit pour mettre des exemplaires de cette thèse à la disposition des personnes intéressées.

L'auteur conserve la propriété du droit d'auteur qui protège sa thèse. Ni la thèse ni des extraits substantiels de celle-ci ne doivent être imprimés ou autrement reproduits sans son autorisation.

ISBN 0-315-65340-X

## Abstract

Experimental procedures and results from ice indentation programs conducted by Mobil Oil Canada at Pond Inlet (1984) and by Memorial University of Newfoundland on Hobson's Choice Ice Island (1989) are detailed. Both field programs utilized a hydraulically powered servo-controlled indentation system with a series of spherical and flat indenters. Nominal contact areas in the experiments ranged from 0.02 m<sup>2</sup> to 3.0 m<sup>2</sup>. The most significant observation in the testing programs was the development of a dynamic load-time trace, i.e., ice-induced vibrations, with frequencies in the area of 30 Hz. Alternate pulverization of ice and clearing (extrusion) of crushed ice products from the impact zone is suggested as the primary mechanism for the observed dynamics, consistent with previous research.

The Pond Inlet and Ice Island data sets are examined with emphasis on the behavior of crushed ice during the extrusion cycle and its importance to the overall dynamic process, including crushed ice layer thickness, impact area reduction by spalling, and dynamic response spectra. Crushed ice layer thickness is observed to vary across the impact zone and, together with highly variant local pressures, suggests that crushing and extrusion takes place in localized areas. These high pressure zones, or "hot spots", vary both spatially and temporally and make it difficult to infer a pressure distribution across the entire impact zone. Rather, the impact area may be thought of as a collection of small hot-spots (high pressure zones) linked by a matrix of highly damaged or pulverized ice under low pressure.

Loads and pressures observed in the experiments are simulated by treating crushed ice as an incompressible linear viscous fluid during the extrusion cycle. Simulation of load and central pressure for a spherical patch loading case is discussed in greatest detail and a body of data is developed for an indentation test which exhibited dynamic behavior in both load and central pressure. Examples of a two-dimensional incremental analysis for irregular crushed ice layer thickness profiles and extrusion over a three-dimensional elliptical contact zone are also presented.

## Acknowledgements

The author is greatly indebted to Dr. Ian Jordaan, NSERC/Mobil Industrial Research Professor in Ocean Engineering, Memorial University of Newfoundland, for his helpful suggestions and guidance throughout the course of this work. A special thanks also to Dr. Richard McKenna for his generous assistance and numerous helpful discussions in various aspects of ice engineering.

Results of the Pond Inlet experiments were generously made available by Mobil Oil Canada Properties. The assistance of Mr. Wes Abel and Mr. Doug Goodridge in this regard is gratefully acknowledged. The continuing encouragement and interest in this and related projects by Dr. Robert Frederking, National Research Council Canada, and Dr. Derek Muggeridge, Chairman, Ocean Engineering Research Centre, Memorial University, is greatly appreciated. Thanks also to Mr. Barry Stone, Memorial University, for his helpful comments and suggestions.

Development and application of viscous models for crushed ice extrusion owes greatly to the work of Dr. Marc A. Maes, Queen's University. His assistance in all aspects of the models presented herein is greatly appreciated.

Financial support for this work was provided by the Natural Sciences and Engineering Research Council of Canada (NSERC), Petro-Canada Resources Limited, and the Centre for Cold Ocean Resources Engineering (C-CORE). The courtesy and generosity of these organizations is gratefully acknowledged.

# Contents

List of Figures	iv
List of Tables	vii
Nomenclature	viii
<b>1 Introduction and Scope</b>	<b>1</b>
<b>2 Ice-Induced Vibration of Structures</b>	<b>6</b>
2.1 Field Observations . . . . .	7
2.1.1 Bridge Piers . . . . .	7
2.1.2 Lightpiers and Navigational Aids . . . . .	8
2.1.3 Offshore Structures . . . . .	10
2.2 Damage and the Ice Crushing Process . . . . .	14
2.3 Crushed Ice Behaviour . . . . .	17
2.4 Indentation and Local Pressure . . . . .	19
<b>3 Medium-Scale Ice Indentation</b>	<b>21</b>
3.1 Indentation Apparatus . . . . .	22
3.2 The Pond Inlet Experiments (1984) . . . . .	26
3.2.1 Test Plan . . . . .	26
3.2.2 Main Results . . . . .	32
3.3 Ice Island Field Program . . . . .	37
3.3.1 Equipment Description . . . . .	37
3.3.2 Site Selection . . . . .	39
3.3.3 Test Preparation . . . . .	43
3.3.4 Test Plan . . . . .	46
3.3.5 Main Results . . . . .	48
3.3.6 Ultrasonic Measurements . . . . .	49
3.4 Equipment Performance . . . . .	53

<b>4</b>	<b>Indentation Analysis</b>	<b>55</b>
4.1	Crushed Layer Thickness . . . . .	55
4.1.1	Ultrasonic Measurements . . . . .	62
4.2	Sieve Analysis . . . . .	63
4.3	Spalling and Impact Area Reduction . . . . .	66
4.4	Dynamic Characteristics . . . . .	71
4.4.1	Test Start-Time . . . . .	72
4.4.2	Response Spectra . . . . .	74
4.5	Pressure Distributions . . . . .	78
<b>5</b>	<b>Extrusion Simulation</b>	<b>80</b>
5.1	Spherical Patch Model: Viscous Flow . . . . .	82
5.2	Variable Layer Thickness . . . . .	89
5.2.1	Incremental Analysis of Irregular Layers . . . . .	89
5.3	Three-Dimensional Extrusion . . . . .	93
<b>6</b>	<b>Simulation Results and Discussion</b>	<b>96</b>
6.1	Spherical Patch Loading . . . . .	97
6.1.1	Layer Thickness Estimates . . . . .	97
6.1.2	Crushed Ice Viscosity . . . . .	99
6.1.3	Contact Area Reduction . . . . .	100
6.1.4	Simulation Results . . . . .	102
6.1.5	Discussion . . . . .	109
6.2	Variable Layer Thickness . . . . .	113
6.2.1	Discussion . . . . .	117
6.3	3-D Extrusion . . . . .	119
6.3.1	Discussion . . . . .	123
<b>7</b>	<b>Conclusions and Recommendations</b>	<b>128</b>
	<b>References</b>	<b>128</b>
	<b>Appendix A: Pond Inlet (1984) Data Summary</b>	<b>133</b>
	<b>Appendix B: Ice Island (1989) Data Summary</b>	<b>145</b>
	<b>Appendix C: Approximation for Small <math>\theta_c</math></b>	<b>149</b>

## List of Figures

2.1	Load-time Records for Hondo and Pembridge Bridge Pier Ice-Structure Interactions . . . . .	9
2.2	Typical Offshore Navigational Structure . . . . .	11
2.3	Idealization of Shear Damage (in Plan) for Freshwater Indentation Test . . . . .	15
2.4	Typical "Sawtooth" Dynamic Response for a Rigid Indenter. . . . .	17
3.1	Four-Actuator Indenter System . . . . .	25
3.2	Artist's Conception of the Pond Inlet (1984) Iceberg Indentation Experiments . . . . .	27
3.3	Pressure Cell Locations for Pond Inlet (1984) 0.5 m <sup>2</sup> and 3.0 m <sup>2</sup> Indenters . . . . .	31
3.4	Normalized Pond Inlet (1984) Pressure-Area Relationship . . . . .	33
3.5	Typical Load-Time Records from Pond Inlet (1984) Indentation Experiments T4T1 (1.0 m <sup>2</sup> ) and T4T3 (3.0 m <sup>2</sup> ). . . . .	35
3.6	Ice Island (1989) Indenter Geometry and Layout of the Pressure Cells. . . . .	40
3.7	Test Location and Other Relevant Centres for the 1989 Ice Island Indentation Test Program. . . . .	42
3.8	Schematic of Hobson's Choice Ice Island (1989) . . . . .	45
3.9	Shaped Multiyear Ice Trench Walls (in Plan) Required for Ice Island Field Program (1989). . . . .	47
3.10	Typical Load-Time Records for Hobson's Choice Ice Island (1989) Indentation Test Program. . . . .	50
3.11	Conceptual Arrangement for Ultrasonic Detection of Crushed Ice and Intact Ice Interface, Ice Island (1989). . . . .	51
3.12	Hypothetical Results of Ultrasonic Measurements. . . . .	52
4.1	Typical Indenter Ice Imprint . . . . .	56
4.1	(continued) . . . . .	57

4.2	Digitized Crushed Ice Layer Thickness Profiles of the Pond Inlet (1984) Indentations . . . . .	59
4.3	Results of the Ultrasonic Crushed Ice Layer Detection Trial, Ice Island (1989) Test Number NRC01. . . . .	64
4.4	Composite Gradation Curve of Crushed Ice Particles from the Ice Island (1989) Indentation Tests. . . . .	65
4.5	Theoretical Reduction of Contact Area by Spalling. . . . .	68
4.6	Hypothetical Size Effect Resulting from Spalling. . . . .	69
4.7	Observed Size Effect from Pond Inlet (1984) Data Set. . . . .	69
4.8	Center and Prorated Average Pressure: Pond Inlet (1984) 1.0 m <sup>2</sup> Test Number T2T6. . . . .	70
4.9	Synchronization of Data Traces for Analysis . . . . .	73
4.10	Typical Response Spectra for Medium-Scale Indentation. . . . .	75
4.10	(continued). . . . .	76
4.11	Frequency vs. Indenter Velocity for Pond Inlet (1984) 1.0 m <sup>2</sup> and 3.0 m <sup>2</sup> Tests. . . . .	78
5.1	Spherical Patch Indentation of an Ice Mass. . . . .	83
5.2	Incremental Analysis of Irregular Crushed Ice Layer. . . . .	91
5.3	Two-Dimensional Extrusion Between Flat Parallel Plates. . . . .	91
6.1	Section of Load-Displacement Trace: Pond Inlet T2T6 (1.0 m <sup>2</sup> ). 99	
6.2	Sensitivity of Load vs. Crushed Ice Layer Thickness to Crushed Ice Viscosity. . . . .	101
6.3	Sensitivity of Load and Pressure vs. Area Reduction to Crushed Ice Viscosity. . . . .	103
6.4	Sensitivity of Load and Pressure vs. Crushed Ice Layer Thickness to Area Reduction Factor. . . . .	104
6.5	Simulation Results (0.5 m <sup>2</sup> ): Pond Inlet Test Number T2T1. . . . .	106
6.6	Simulation Results (1.0 m <sup>2</sup> ): Pond Inlet Test Number T2T6. . . . .	107
6.7	Pond Inlet T2T6 (1.0 m <sup>2</sup> ): Total Load and Center Pressure Traces. . . . .	108
6.8	Contact Area vs. Indenter Velocity for the Spherical Patch Simulation of Pond Inlet Test Number T2T6 (1.0 m <sup>2</sup> ). . . . .	112
6.9	Two-Dimensional Incremental Analysis Examples . . . . .	114
6.9	(continued) . . . . .	115
6.9	(continued) . . . . .	116
6.10	Incremental Analysis Simulation Results for Ice Island Test NRC08. . . . .	118
6.11	Typical Pressure Distributions for 3-D Extrusion Simulation. . . . .	120

6.12	Pressure Traces, Pond Inlet 3.0 m <sup>2</sup> Test Number T1T5 for Pressure Cells P1 Through P5. . . . .	122
6.13	Relevant Load-Time Trace, Pond Inlet Test Number T1T5 (3.0 m <sup>2</sup> ). . . . .	123
6.14	3-D Viscous Extrusion Simulation Results for Pond Inlet Test Number T1T5 (3.0 m <sup>2</sup> ). . . . .	124

## List of Tables

3.1	Pond Inlet Impact Parameters . . . . .	28
3.2	Pond Inlet Indentation Test Matrix. . . . .	30
3.3	Pond Inlet Indenter Instrumentation. . . . .	32
3.4	Pond Inlet Pressure Cell Records. . . . .	36
3.5	Ice Island Indenter Instrumentation. . . . .	39
3.6	Test Matrix: Ice Island Indentation Program (1989). . . . .	48
4.1	Crushed Ice Layer Thickness Observations Derived from Photographs of the Pond Inlet (1984) Indentations. . . . .	61
4.2	Area Reduction by Spalling Derived from Photographs of the Pond Inlet (1984) Indentation Tests. . . . .	67
4.3	Response Spectra Summary for the Pond Inlet (1984) and Ice Island (1989) Load-Time Records. . . . .	77
6.1	Pond Inlet T2T6: Extrusion Simulation Results. . . . .	110
A.1	Pond Inlet Pressure Cell Data. . . . .	144

# Nomenclature

$\rho$	density of crushed ice ( $\text{kg/m}^3$ )
$\vec{v}$	velocity field (m/s)
$R$	radius of curvature (m)
$p$	pressure (MPa)
$\mu$	dynamic viscosity (MPa·s)
$t$	time (s)
$\omega$	frequency (Hz)
$\vec{\nabla}$	gradient vector
$\nabla^2$	the Laplacian operator
$v_r$	radial component of velocity
$v_\theta$	tangential component of velocity
$\ell$	crushed layer thickness (mm)
$v_o$	indenter velocity (m/s)
$F$	total load or force (MN)
$h$	viscous layer thickness (mm)
$v_o$	indenter velocity
$\bar{p}$	average pressure (MPa)
$\bar{u}$	average velocity in x-direction (mm/s)
$n$	number of nodes
$\theta$	angle (radians)
$\theta_t$	angle to edge of contact zone
$e$	eccentricity of ellipse
$K$	velocity profile constant
$a$	one-half ellipse major axis length
$b$	one-half ellipse minor axis length
$\gamma$	crushed ice layer profile parameter
$h_o$	layer thickness at center of ellipse
$R$	elliptical area parameter

# Chapter 1

## Introduction and Scope

Economical development of the offshore resources of arctic and sub-arctic regions is one of the greatest engineering challenges of recent times. Frigid temperatures coupled with ice in its many forms makes the arctic one of the harshest environments for offshore activity. Impact of ice has been recognized as an important loading condition on arctic offshore facilities since the first such structure was commissioned in Cook Inlet, Alaska in the 1960's. Since that time, offshore petroleum discoveries in the Canadian arctic and east coast have led to an increased interest in the loads generated by the interaction of ice and structure.

Ice loads on an offshore structure make take numerous forms. An ice sheet may fail in pure crushing, flexure, buckling, splitting, or a combination of these modes. Highest ice loads are generally manifested through pure crushing or pulverization of the ice sheet into a mass of very small discrete particles near the contact zone. The actual failure mode experienced in an ice-structure interaction is directly related to the properties of the ice

sheet and the physical characteristics of the structure itself. For example, an ice feature which impacts a vertical circular cylindrical pier at high speed typically fails in the crushing mode, whereas a sloping or conical indenter instigates bending failure (resulting in comparatively lower loads).

Arctic engineering experience has shown that interactions of ice features with offshore structures are often accompanied by regular structural vibrations. Known as "ice-induced vibrations", this dynamic behaviour was prevalent during extended periods of crushing failure and was not considered threatening to overall structural stability. The actual extent and effects of full-scale ice-induced vibrations were clearly demonstrated in practice in 1986, when the *Molikpaq* Mobile Arctic Caisson (MAC) experienced severe vibrations under the impact of a large ice floe. Crushing failure against the near-vertical sides of the MAC created an extended period of severe vibrations and caused a portion of the sand core of the *Molikpaq* to liquefy. Structural stability was compromised by a corresponding loss of lateral strength.

The *Molikpaq* incident illustrated the importance of ice-induced vibrations in the design and operation of arctic offshore facilities. Dynamic, not static, loads were recognized as potentially critical in ice-structure interactions and may even represent the design loading condition. New experimental programs were designed and existing data sets reassessed in order to shed light on the ice crushing process and its role in the observed dynamics. Although small-scale laboratory investigations are very important in this regard, the tendency for ice pressures and loads to decrease with increasing contact area,

known as the scale effect, hampers extrapolation of these results to full-scale interactions. On the other hand, full-scale measurement programs are expensive and difficult to co-ordinate from a research perspective.

In 1984, an ambitious field program was commissioned by the Hibernia Joint Venture Participants led by Mobil Oil Canada as operator. A series of high-speed ice indentation tests were performed under controlled conditions on a grounded iceberg near the village of Pond Inlet, Baffin Island in the Northwest Territories, Canada. The experiments were originally designed to specify design criteria for potential iceberg impacts with production structures in the Hibernia field and to investigate the phenomenon of scale effect. Contact areas in the test series ranged from  $0.02 \text{ m}^2$  to  $3.0 \text{ m}^2$ , such that the experiments may be considered "medium-scale" indentation tests, as opposed to laboratory (ice tank) experiments or full-scale (*Molikpaq*) studies. One of the most interesting results from the Pond Inlet field program was the presence of very regular vibrations in the high-speed ice impacts, accompanied by the pulverization of ice into a pasty mass of crushed particles. In light of the dynamic activity observed on the *Molikpaq*, these results represent an excellent data set for the analysis of ice-structure interaction. Another series of indentation tests was performed by Mobil Oil Canada in 1986 on multiyear ice in the Canadian Arctic, but the results are proprietary.

In 1987, Mobil Oil Canada Properties, on behalf of the Hibernia Joint Venture Participants, donated the ice indentation system used in the Pond Inlet experiments to Memorial University of Newfoundland. At the same

time, the results of the Pond Inlet test series were released to the Ocean Engineering Research Centre, Memorial University of Newfoundland, on a confidential basis. Direct access to both the indentation equipment and the results of the Pond Inlet test series enabled Memorial University to further investigate ice-induced vibrations. A new ice indentation field program, held on "Hobson's Choice" Ice Island in the Canadian Arctic Ocean in the spring of 1989, was conceived to complement the Pond Inlet data set. The behaviour of crushed ice and its role in the development of structural vibrations was identified as the thrust of the research program.

Details of the medium-scale ice indentation experiments conducted on the Ice Island (1989) and in Pond Inlet (1984) are presented herein. Emphasis is placed on Memorial University's Ice Island program from a planning and logistical viewpoint, though the Pond Inlet data set is more complete and better suited to modelling. Crushed ice, which plays a critical role in the observed dynamics of the high-speed tests, is investigated in detail. Salient features of the indentation zone and observations of load and pressure are utilized in modelling the thin layer of crushed ice as a viscous material. Specifically, the scope of this work may be categorized as follows:

1. Literature survey of field observations of ice-induced vibrations, including recent ice failure theories and the behaviour of crushed ice products.
2. Description of medium-scale ice indentation experiments performed in Pond Inlet (Mobil Oil Canada, 1984) and on Hobson's Choice Ice Island (Memorial University and others, 1989); presentation of the major

findings of both testing programs.

3. General analysis of the indentation experiments with an emphasis on observations of crushed ice behaviour, impact area reduction by spalling, and dynamic characteristics.
4. Simulation of observed loads and pressures based on the treatment of crushed ice as a linear viscous material.
5. Discussion of major findings and recommendations for further research and analysis.

Ultimately, this work is intended to contribute to the development of practical, manageable ice load models for design purposes.

## Chapter 2

# Ice-Induced Vibration of Structures

A general consensus exists in the ice engineering community regarding the dynamic activity that often accompanies ice-structure interactions. Cyclic variations in ice load are attributable to crushing of ice against a structure followed by extrusion of the crushed ice products from the impact zone as the indenter (or the ice) advances. This process has been observed in both field and laboratory programs and is the subject of a considerable body of research.

The mechanics of ice-structure interaction are undeniably complex and the actual process of ice crushing has yet to be resolved. Extensive micro-cracking of ice under load is an important factor in complete pulverization, while the behaviour of the crushed ice products governs, in part, the observed dynamics.

## 2.1 Field Observations

### 2.1.1 Bridge Piers

Incidents of ice damage to bridge piers in Russia have been documented since the late nineteenth century (Korzhasin, 1962) while the first Canadian reports of such damage involved a bridge in Québec (Leonard, 1898). Since then, numerous research programs have generated a considerable amount of data on the interaction of ice with both rigid and flexible bridge piers. A general trend resulted from large-scale bridge pier observations: actual ice loads were much less than those prescribed by relevant design codes and standards.

An indepth program of ice force data collection from rivers in Alberta was initiated in 1967 by the Transportation and Surface Water Engineering Department of the Alberta Research Council and represents one of the most complete data sets of this type. Although data collection was sparse on most of these bridges, recorded ice pressures were much less than design code specifications. Two bridges monitored during the program, at Hondo on the Athabasca River and Pembridge on the Pembina River, yielded detailed and important information on the dynamic nature of ice failure by crushing.

Vibrations induced by ice crushing were evident throughout the Hondo Bridge field program, although most ice failures were by bending, splitting or some combination of these processes. It has been clearly demonstrated that the dynamics observed at the Hondo site are not related to the natural

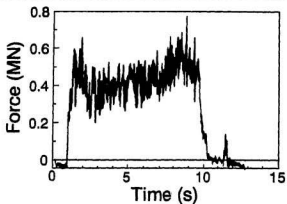
frequency of the pier-load cell mechanical system. The significant frequencies of the ice-induced oscillations were in the range of 15-20 Hz, while the natural frequency of the pier-load cell system was initially reported as 100 Hz (Sanden and Neill, 1968) and re-evaluated as 57 Hz (Gordon and Montgomery, 1981). Either estimate precludes resonant effects. The massive bridge piers were also very stiff, such that the observed vibration frequencies may be attributed to the failure of the ice alone.

The Pembridge measurement system consisted of a specially constructed vertical steel pile with a fundamental frequency in the range of 12-14 Hz (Gordon and Montgomery, 1981). It has been demonstrated that ice-induced oscillations at Pembridge may have significant frequency components in the 5-30 Hz range, resulting in magnification of those frequencies in the 12-14 Hz range (Michel, 1978). Typical load-time traces for events at both Hondo and Pembridge are presented in Figure 2.1 and the dynamic features are clearly evident.

### **2.1.2 Lightpiers and Navigational Aids**

The vibratory effects of ice interaction have been well-documented from the experience of navigational aids such as lighthouses and channel markers in North America and, to a greater extent, in Northern Europe. These structures may be thought of as vertical indenting piers cantilevered from the seabed. Global wave and ice loads are minimized by employing a small diameter at the water-plane, but the narrow diameter generally results in the crushing failure of ice. The cantilever design of many of the structures facil-

HONDO BRIDGE PIER ICE-STRUCTURE INTERACTION  
*(from Gordon and Montgomery, 1981)*



PEMBRIDGE PIER ICE-STRUCTURE INTERACTION  
*(from Gordon and Montgomery, 1981)*

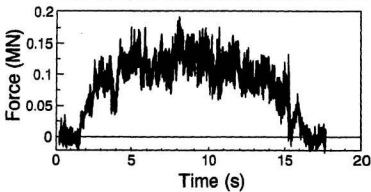


Figure 2.1: Load-time Records for Hondo and Pembridge Bridge Pier Ice-Structure Interactions (*Gordon and Montgomery, 1981*).

itates resonant vibrations under the continuous attack of a large ice sheet or the impact shock of a discrete ice feature. Accelerations associated with the vibrations are usually greatest near the top of the structure and may affect the performance of lantern equipment or create an uncomfortable working environment on manned lightpiers.

Numerous navigational aids have been installed in the northern Baltic, including lighthouses, lightpiers (somewhat smaller than lighthouses), and channel markers. A typical structure is illustrated in Figure 2.2. Extreme vibrations were observed by service personnel on the Norströmsgrund lighthouse in the Gulf of Bothnia under the action of drifting ice. A structural defect was first suggested as the cause of the severe shaking, but subsequent analysis indicated that the facility was resonating as it cut through the ice sheet (Engelbrektsen, 1977). Similarly, severe vibrations were observed in the Kemi I lighthouse, a tubular steel pile driven into the seabed in the northern Gulf of Bothnia, under the attack of even very thin ice sheets. The structure eventually collapsed in the spring of 1974 during its first operational season, most likely the result of an impact with a pressure ridge (Määttänen, 1977 and 1975). The original Kemi I was replaced with a bottom-founded concrete-caisson tower equipped with a variety of instruments to further investigate ice-structure interactions.

### **2.1.3 Offshore Structures**

Petroleum exploration in arctic and sub-arctic environments is a relatively recent endeavour. Examples of ice-induced vibration on full-scale offshore

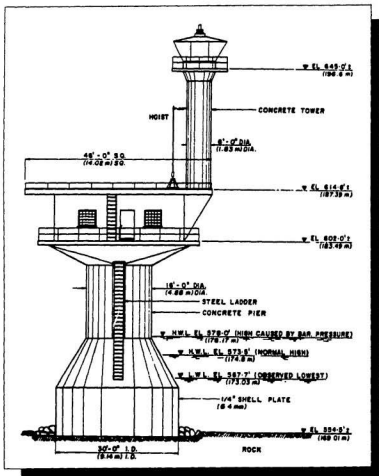


Figure 2.2: Typical Offshore Navigational Structure (Danys, 1977).

structures are therefore limited but demonstrate the importance of dynamic ice loads in design. Peyton (1966, 1968) reported vibrations associated with the crushing failure of ice against the circular legs of drilling platforms in Cook Inlet, Alaska. Vibration frequency was in the range of 1-10 Hz. Subsequent analysis of Cook Inlet ice force data by Blenkarn (1970) confirmed this so-called "ratcheting" behaviour but disputed Peyton's claim that ice exhibits a clearly-defined failure frequency of approximately 1 Hz.

Field measurements of dynamic ice loading on a six-legged, steel jacket platform in the Bo-hai Gulf, northern China, were reported by Jizu (1981). The platform, used for accommodations and miscellaneous equipment, was "... shaken violently" by drifting ice in the area. A representative ice-induced vibration frequency of approximately 2 Hz was observed. During the event, a nearby flare jacket collapsed, later attributed to a piling failure below the mudline (Janbu et al., 1983).

A series of indentation tests were performed on freshwater lake ice in the late 1970's as reported by Kry et al. (1978). A 1.2 meter diameter semi-cylindrical indenter was used to penetrate 250 mm thick ice sheets on Eagle Lake, Alberta. In the higher velocity tests (penetration rates approaching 10 mm/s), a dynamic response was observed during failure modes termed "ductile flaking" and "brittle flaking". The brittle flaking process yielded smaller fragments of ice and lower peak stresses than ductile flaking and

occurred exclusively in the high-speed tests.

Pilkington et al. (1983) described an ice instrumentation system employed on the vertical-sided Tarsiut caisson-retained artificial islands in the landfast ice zone of the Canadian Beaufort Sea. Significant load transmissions through the ice rubble field surrounding the structure were observed. High-speed crushing of ice against the structure or significant dynamic activity were not reported. Full-scale impact experiments were conducted at Hans Island in the Kennedy Channel west of Greenland in 1980, 1981 and 1983. Deceleration of ice floes impacting the small island were recorded and used to determine the global ice forces and pressures (Metge et al., 1981; Danielewicz and Blanchet, 1988). Although force variations were observed, the interactions were complex and exhibited several modes of failure. The Hans Island test series was a landmark in the development of new design methodologies for arctic structures, illustrating that full-scale global ice loads were generally less than 1 MPa.

The most dramatic example of ice-induced vibration is that of the *Molikpaq* Mobile Arctic Caisson (MAC), deployed at the Amaulikag I-65 site in the Canadian Beaufort Sea. While cutting through a 2 km<sup>2</sup> ice floe on April 12, 1986, crushing failure against the near-vertical sides of the MAC created an extended period of severe vibrations. A portion of the sand core of the *Molikpaq* liquefied and the lateral stability of the structure was seriously compromised. A complete description of the *Molikpaq* and a detailed account of the ice loading event is given by Jefferies and Wright (1988). Of particular

interest in this event was the evidence of a "phase lock" phenomena, a series of non-simultaneous failure events which synchronize in time to produce very regular cyclic load variations across the entire contact width.

## 2.2 Damage and the Ice Crushing Process

It is evident from the previous discussion that the dynamics associated with ice-structure interactions are most pronounced when ice fails in the crushing mode. The ice crushing process is complex and much theoretical and experimental work has been undertaken to study the processes that cause crushing failure. Progressive degradation of ice under load may be termed "damage", and analysis of the physical behaviour of the resulting damaged material is known as "continuum damage mechanics", a relatively new area of research. Damage mechanics has been recognized as one of the most encouraging methods of analysis of the ice crushing process.

Rheologically, ice may be considered an elastic, creeping solid, yet its pronounced brittleness results in a propensity to fracture under load. This behaviour tends to dominate the ever-present creep, particularly during rapid indentation (high strain rates). Triaxial compression testing is one of the most important laboratory tests for ice and has yielded interesting and important results as to the behaviour of ice under load, e.g., Jones (1982). This approach was furthered by Stone et al. (1988) in the analysis of a series of triaxial compression experiments which utilized the degradation of Young's

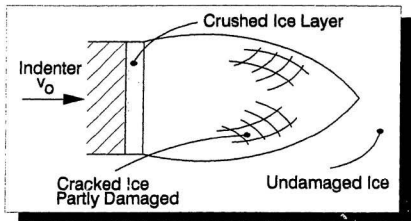


Figure 2.3: Idealization of Shear Damage (in Plan) for Freshwater Indentation Test (Jordaan and Timco, 1988).

Modulus as an assessment of damage.

Microcracks as damage were analyzed by Jordaan and Timco (1988) based on ice sheet indentation experiments reported by Timco (1986). Under compressive states of stress with moderate confining pressures, damage results in a zone of crushed ice near the indenter and a network of very fine microcracks further back within the relatively intact ice. An idealization of the process presented by Jordaan and Timco (1988) is reproduced in Figure 2.3 and suggests that the cracks follow the lines of maximum shear. Jordaan and Timco (1988) adopted a definition of damage whereby pulverization results from a degradation of the shear modulus.

As the load progresses during indentation, microcracks coalesce to form discrete ice particles which may then move with respect to each other. The

product of this progressive degradation is crushed ice and behaves in a manner distinctly different from that of the virgin material. Crushed ice is squeezed out or extruded from the contact zone as the indenter (or ice sheet) advances. The load builds up once again until a new zone of damaged ice pulverizes. In general, a dynamic force cycle in a high-speed indentation is characterized by a gradual increase in load followed by localized failure of the ice mass, resulting in a sudden drop in load. The load gradually increases again during clearing of the crushed ice products until the load is sufficient to pulverize a new zone, and the cycle repeats. This activity is characterized by the classic sawtooth response of Figure 2.4. The very steep load drop is typical of rigid indenters, i.e., elastic rebound of both indenter and ice is insignificant and clearing of crushed ice particles occurs as the load increases (Jordaan and Timco, 1988). If contact area increases during the indentation, a steady increase in load is also observed.

It is important to note that crushed ice may not remain a mass of discrete particles during the interaction. It has been recently suggested that sintering or solidification may occur within the crushed ice zones, yielding a material capable of supporting very high loads. Under high pressures developed in indentation, this material may be considered as a fluid with very high viscosity. An understanding of the behaviour of the crushed ice continuum is important in any analysis of high-speed indentation.

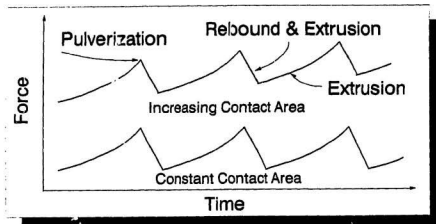


Figure 2.4: Typical "Sawtooth" Dynamic Response for a Rigid Indenter.

### 2.3 Crushed Ice Behaviour

Crushed ice as a viscous material was proposed by Kheisin and Cherepanov (1970) in the analysis of the damaged zone developed in drop-ball ice impact experiments. Hemispherical indenters with mass up to 300 kg were impacted on a freshwater ice cover at velocities up to 6 m/s. The resulting shattered ice material, described as pasty or powdery, developed in a thin intermediate layer between the indenter and the intact ice mass. A distinct interface existed between this zone of crushed ice and the less damaged intact ice below. These results suggested that high-speed impacts generate a distinct, localized zone of pulverized ice with submicroscopic ice particles acting as a lubricant for the matrix of larger crushed ice particles. Following the formation of the crushed ice layer, the advancing indenter causes further damage and the extrusion of this crushed ice layer. Kheisin and Cherepanov (1970) suggested

modelling the crushed ice layer "... as a very viscous Newtonian liquid" and this approach was later adopted by Kurdyumov and Kheisin (1976) in an analysis of Kheisin and Cherepanov's experiments. Both viscous and plastic terms were included in an axisymmetric analysis of the observed crushed ice layer, though the plasticity term was later found to be negligible in comparison to the viscous effects. Inertial forces were not considered and elastic deformations were deemed insignificant. Results of the model utilized crushed layer viscosities in the 10 kPa-s to 100 kPa-s range and compared well to the original drop ball experiments. The model was not considered applicable to all cases of ice-structure interaction and in a review of ship-ice interactions, Tunik (1989) concludes that practical application of the Kurdyumov-Kheisin model to full-scale interactions remains limited by a lack of experimental data.

Assuming crushing failure, Nevel (1986) developed an iceberg impact force model based on viscous theory. The Navier-Stokes equations governing the behaviour of crushed ice as a viscous material were applied for the case of a thin layer between an indenter and intact ice mass. The modelling of crushed ice as a granular material has been proposed by Hallam and Pickering (1988) and utilizes the well known Mohr-Coulomb failure criterion originally developed for soils. The behaviour of crushed ice was also studied in a series of experiments reported by Finn et al. (1989). Laboratory prepared crushed ice was placed between two flat instrumented plates and the ice extruded or squeezed out from between the plates at various velocities. A similar experimental series on crushed ice extrusion was carried out by Geotechni-

cal Resources Limited (1986). Results of both experimental programs are proprietary.

## 2.4 Indentation and Local Pressure

The design of structural members for arctic offshore facilities is based on local ice loads experienced by small contact areas. Remarkably high ice pressures (up to 40 MPa) developed in full-scale icebreaker trials were reported by Glen and Comfort (1983) with the observation that these pressures were uneven across the contact surface. Very high local pressures have also been reported during ice interactions with exploration and production structures in the Beaufort Sea. These local pressures are considerably higher than the laboratory uniaxial compressive strength of ice, due in part to high confinement in the contact zone. Iyer (1989) refers to these areas of high local pressure as "hard spots", zones within the global nominal contact area in which a maximum pressure may occur. The development of these zones of intense local pressure makes it unlikely that a uniform pressure distribution exists across the nominal contact area. Riska (1987), for example, recognized the variability and irregularity of ice contact in the development of an interaction model between sea ice and an icebreaker hull.

Iyer (1989) makes the connection between full-scale observations of local ice pressures and controlled indentation experiments. The pressure developed in the nominal contact zone of an indentation test is analogous to the global ice loading condition experienced in arctic structures. Pressure max-

ima arise throughout the nominal contact area resulting in a non-uniform pressure distribution across the face of the indenter. Controlled, high-speed ice-structure interactions may be therefore typified by irregular pressure distributions and very high local maxima. Progressive damage, pulverization, and extrusion of crushed ice in localized zones play a significant role in the observed phenomenon.

## Chapter 3

# Medium-Scale Ice Indentation

Laboratory investigations such as triaxial compression tests or ice tank indentations may be generally classified as small-scale experiments. Extrapolation of these data sets to full-scale arctic structures has proven difficult since contact areas may be hundreds of times greater. Loads derived from small-scale studies have considerably overestimated actual global ice loads observed in the field. Full-scale experiments on prototype structures would be ideal, but the cost involved is often prohibitive. The ice indentation system commissioned by Mobil Oil Canada in 1984 and donated to the Ocean Engineering Research Centre, Memorial University in 1987, appears to fill the gap between laboratory tests and full-scale prototype studies. Contact areas ranged from  $0.02 \text{ m}^2$  to  $3.0 \text{ m}^2$  and may therefore be considered "medium-scale" indentations. The  $3.0 \text{ m}^2$  indentations may also approach contact areas developed in full-scale ice-structure interactions.

Details of the indentation experiments conducted by Mobil Oil Canada at Pond Inlet, N.W.T. (1984) and by Memorial University on Hobson's Choice Ice Island (1989) are presented hereafter. The indentation equipment remained essentially the same for both experimental programs, although in the Pond Inlet test series larger indenters and the full capacity of the hydraulic system were used. In terms of contact area and indenter power, the Pond Inlet experiments are more complete than that of the Ice Island testing program. Local pressure measurements in the latter test series are very valuable, however. As the author was directly involved in the planning and logistics of the 1989 Ice Island field program, this test series is described in greater detail.

### **3.1 Indentation Apparatus**

In 1983, Geotechnical Resources Limited of Calgary, Alberta (Geotech) was contracted by the Hibernia Joint Venture Participants (Mobil Oil Canada Limited, operator) to design and construct a controlled indentation system which simulated the impact between a massive ice feature and a rigid structure. Development of a system which could produce the required loads in a controlled manner was a formidable task: the system must be powerful yet manageable. Geotech recognized this priority in their design philosophy for the indenter and concluded that the complete system must withstand ice impact, have minimum weight and dimensions for mobility purposes, require a minimum of assembly in the field, and be versatile with future testing

programs in mind (Geotech Arctic Services, 1985).

The indentation system consists of a spherical indenting surface, actuator, and flexible base plate combination mounted on a steel skid of beam and strut construction. Skids were constructed for both the single and quad-actuator arrangements for ease of movement in the field. A 1.0 m<sup>2</sup> back plate behind each actuator distributed the load from that actuator to a flat ice surface, ensuring that ice would not fail in that region. Hydraulic power was provided to the actuators by a massive accumulator bank capable of delivering approximately 18,500 MN at full capacity (four-actuator system). Five spherical indenters with differing radii of curvature were machined with nominal surface areas ranging from 0.02 m<sup>2</sup> to 3.00 m<sup>2</sup>. The spherical shape was selected for its symmetry and to ensure that ice crushing failure would be instigated during indentation. Design ice pressures for the indenters were established based on Geotech's previous experience and pressure-area relationships available in the literature. All indenters were machined from aluminum block and pressed to the desired radius of curvature, though the large 3.0 m<sup>2</sup> indenter was constructed from welded steel elements. The indenters were instrumented with a variety of load and pressure cells, the number and positioning of which depended on indenter dimensions. Complete details of the design of the indenters, actuators, accumulators, skids, and various related items are detailed in the data report prepared for the Hibernia Joint Venture Participants (Geotech Arctic Services, 1985). The final configuration of the indentation system is illustrated in Figure 3.1 and includes four hydraulic actuators for the 3.0 m<sup>2</sup> and 1.0 m<sup>2</sup> indenters, and a single actuator

for the  $0.5 \text{ m}^2$ ,  $0.1 \text{ m}^2$  and  $0.02 \text{ m}^2$  indenters.

Indenter movement was controlled by closed-loop (feedback) methods in which a test variable (output) is continuously monitored and compared to its target value (input). Closed-loop servo-controlled hydraulic systems are commonly used in many aspects of engineering materials testing. Any deviation from the input (command) signal is interpreted by the servo-controller as a cue to drive the actuator in such a way so as to eliminate the error between input and output signals. When a correction is called for, the servo-controller instructs the servo-valve to pump oil in or out of the actuator to compensate. Indenter displacement was selected as the control variable for indenter movement, i.e., indenter displacement would be monitored by pots mounted to the indenter and a fixed surface, and this output signal used as the feedback parameter. All aspects of the indentation tests were digitally controlled and data recorded by computer.

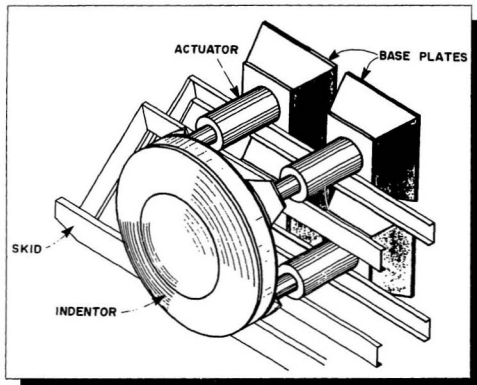


Figure 3.1: Four-Actuator Indenter System (*Geotech Arctic Services, 1985*).

## 3.2 The Pond Inlet Experiments (1984)

Suitable test sites for the proposed indentation experiments required a combination of large quantities of ice and available logistical support. To this end, a grounded iceberg near Pond Inlet on eastern Baffin Island, Northwest Territories, Canada was identified as the ideal site for the experiments. A series of horizontal tunnels were excavated into the ice mass and the indenter system positioned in a tunnel with the spherical indenter and backing plates facing a smooth vertical wall. The complete operation is best illustrated by the schematic of Figure 3.2, where the large 3.0 m<sup>2</sup> indenter mounted on the quad-actuator skid has been placed in a tunnel in preparation for a test. The accumulator skids and data acquisition hut are in the foreground.

### 3.2.1 Test Plan

In order to simulate a potential iceberg impact with an offshore structure, indenter velocity was assumed to vary from some initial maximum to zero, i.e., to represent the "slowing down" of an iceberg after impact. For safety and other reasons, displacement and not velocity was selected as the feedback parameter, although a specific velocity profile was desired for the tests. The velocity profile of the indenter for all tests at Pond Inlet followed the relationship:

$$v(t) = v_0 \cdot \cos(\omega t) \quad (3.1)$$

where  $v$ : indenter velocity (mm/s);

$v_0$ : initial velocity (100 mm/s for all tests);

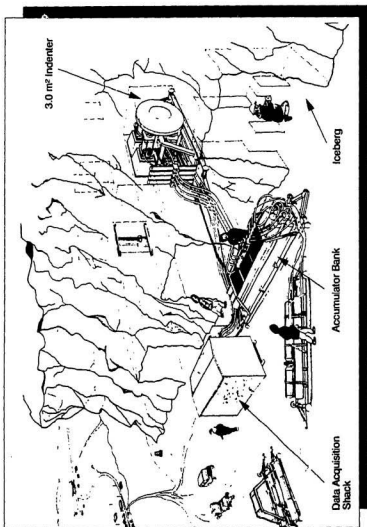


Figure 3.2: Artist's Conception of the Pond Inlet (1984) Iceberg Indentation Experiments (*Geotech Arctic Services, 1985*).

Nominal Indenter Contact Area (m <sup>2</sup> )	R (mm)	$x_o$ (0.1R) (mm)	$\omega$ (cycles/s)	Test Length (s)
3.0	2300	230	0.435	3.61
1.0	1280	128	0.781	2.01
0.5	900	90	1.11	1.41
0.10	400	40	2.5	0.63
0.02	200	20	5.0	0.31

Table 3.1: Pond Inlet Impact Parameters (*Geotech Arctic Services, 1985*).

$\omega$ : frequency (cycles/s); and

$t$ : time (s).

Integration of this velocity profile yielded the displacement command signal:

$$x(t) = x_o \cdot \sin(\omega t) \quad (3.2)$$

where  $x_o$ , the maximum penetration of the indenter into the ice, was fixed at 10% of indenter radius of curvature (R). This resulted in a sinusoid frequency,  $\omega$ , of  $(v_o/x_o)$  or  $\omega = v_o/(0.1R)$ . Relevant impact parameters for the tests are summarized in Table 3.1.

Indentation tests were performed in each of four tunnels carved out of the grounded iceberg. Table 3.2 summarizes the testing schedule and includes the identification tag for each test utilized throughout this document. The spherical indenters used at Pond Inlet were instrumented to varying degrees as presented in Table 3.3. Small pressure cells were incorporated into the face of the 0.5 m<sup>2</sup> and 3.0 m<sup>2</sup> indenters at the locations noted in Figure 3.3.

Other indenters had a single pressure cell in the center of the indenter face.

The general testing procedure as reported by Geotechnical Resources personnel may be summarized as follows (Geotech Arctic Services, 1985):

1. Indenter mounted on actuator and instrumentation installed;
2. Indenter skid positioned in tunnel, aligned, and hoses connected;
3. Displacement pots installed and aligned;
4. All cables connected, data acquisition systems warmed up, and systems calibrated;
5. Indenter brought forward to tunnel wall hydraulically and displacement command signal programmed;
6. Data acquisition started and hydraulics applied;
7. When full hydraulic power attained, command signal triggered and test started.

Following the test, the indenter was relocated and the impact surface examined. Most of the impact areas from the Pond Inlet test series were photographed in plan with a rough scale drawn on the adjacent flat tunnel wall. A cross-section of each impact zone was cut out of the impact zone with chain saws and this profile photographed as well.

Nominal Indenter Contact Area	R (mm)	Tunnel Number	Test Number	Test I.D.
3.0 m <sup>2</sup>	2300	1	5	T1T5
		3	2	T3T2
		4	2	T4T2
		4	3	T4T3
1.0 m <sup>2</sup>	1280	1	4	T1T4
		2	5	T2T5
		2	6	T2T6
		3	1	T3T1
0.5 m <sup>2</sup>	900	4	1	T4T1
		2	1	T2T1
		2	2	T2T2
		3	3	T3T3
0.10 m <sup>2</sup>	400	3	3	T3T3
		3	4	T3T4
		1	2	T1T2
		1	3	T1T3
0.02 m <sup>2</sup>	200	2	3	T2T3
		4	4	T4T4
		4	5	T4T5
		1	1	T1T1
		2	4	T2T4
		3	5	T3T5
		4	6	T4T6

Table 3.2: Pond Inlet Indentation Test Matrix.

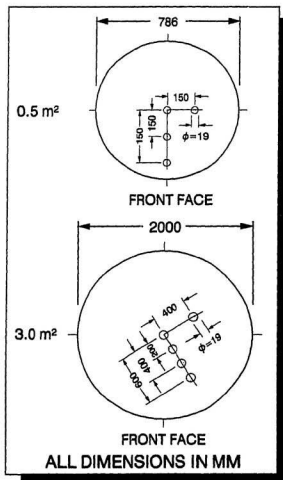
**POND INLET (1984) PRESSURE CELL LOCATIONS**

Figure 3.3: Pressure Cell Locations for Pond Inlet (1984) 0.5 m<sup>2</sup> and 3.0 m<sup>2</sup> Indenters (*Geotech Arctic Services, 1985*).

Instrument	Nominal Indenter Area (m <sup>2</sup> )				
	0.02	0.10	0.50	1.0	3.0
Load cell	3	3	3	4	4
Pressure cell	1	1	4	1	5
Displacement pot	1	1	1	4	4

Table 3.3: Pond Inlet Indenter Instrumentation.

### 3.2.2 Main Results

As previously mentioned, the impetus for the Pond Inlet field program was the investigation of iceberg crushing strengths for design purposes and the confirmation of a pressure-area relationship. Scale effects were analyzed in this regard as reported by Johnson and Benoit (1987) and a pressure-area relationship in which ice pressure decreases with increasing contact area was recognized (Figure 3.4). Complete results from the Pond Inlet field program suggest much more than the effects of scale in an ice-structure interaction. The most significant finding was the dynamic nature of high-speed ice impact.

Typical features and major findings of the Pond Inlet indentation experiments are presented in this section. As there were over 20 complete indentation tests performed with up to 18 data channels monitored per test, presentation of the whole data set would quickly fill up several volumes. Instead, only the load-time traces for the 0.5 m<sup>2</sup>, 1.0 m<sup>2</sup> and 3.0 m<sup>2</sup> tests are included in Appendix A.

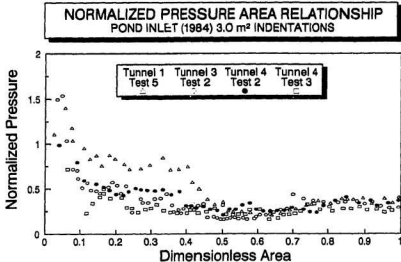


Figure 3.4: Normalized Pond Inlet (1984) Pressure-Area Relationship (*Johnson and Benoit, 1987*).

In general, load-time records (and occasionally pressure-time records) from Pond Inlet exhibit dynamic activity which is spectacular in its regularity and amplitude. The force-time histories for typical 1.0 m<sup>2</sup> and 3.0 m<sup>2</sup> indentation tests are presented in Figure 3.5 and illustrate the phenomenon of ice-induced vibration. In these examples, the classic sawtooth response is evident throughout the entire test length except for the initial stages, where crushing failure has not yet been instigated. As the test winds down and the indenter velocity approaches zero from its initial value of 100 mm/s, the frequency of vibration decreases. For example, vibration frequency in the early stages of the 1.0 m<sup>2</sup> test T4T1 (when indenter velocity is high) is 50 Hz. Near the end of the same test, the vibration frequency is 15 Hz. Dynamic

response is analyzed in detail in Section 4.4.

Videotape records of the Pond Inlet tests show the dramatic ejection of crushed ice from the impact zone as the indenter advances. Photographs of the impact zones after the tests show clearly that a distinct layer of pulverized ice forms during impact. Development and extrusion of crushed ice is an important factor in the overall interaction process.

Pressures developed in the indentations were generally high. Peak and mean values for both a centrally-located pressure cell and the computed average pressure (i.e., total load divided by area), are summarized in Table 3.4. Note that the 0.5 m<sup>2</sup> and 3.0 m<sup>2</sup> tests utilized a series of pressure cells incorporated along the face of the indenter. All other tests utilized a single pressure cell at the geometrical center of the indenter plate. Only one of the four 3.0 m<sup>2</sup> tests had an active pressure cell at the center of the indenter. Peak and mean values for all pressure cells for each Pond Inlet test are tabulated in Appendix A.

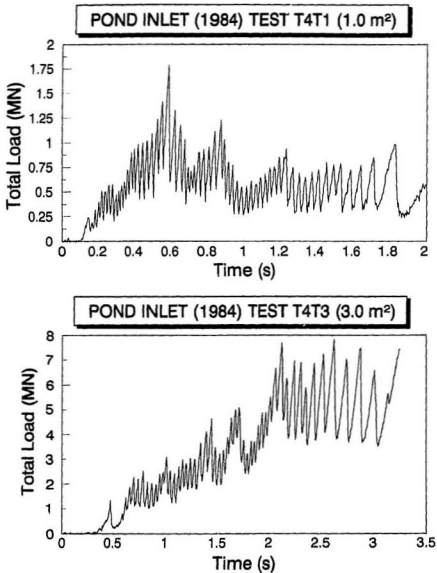


Figure 3.5: Typical Load-Time Records from Pond Inlet (1984) Indentation Experiments T4T1 (1.0 m<sup>2</sup>) and T4T3 (3.0 m<sup>2</sup>).

Size (m <sup>2</sup> )	Test I.D.	Center Pressure		Average Pressure	
		Peak (MPa)	Mean (MPa)	Peak (MPa)	Mean (MPa)
0.02	T1T1	35	13	-	-
	T2T4	44	6	9	2
	T3T5	50	26	7	4
	T4T6	48	13	8	4
0.1	T1T2	37	17	11	6
	T1T3	56	27	12	7
	T2T3	55	30	23	6
	T4T4	56	25	10	3
	T4T5	37	11	8	2
0.5	T2T1	58	19	27	10
	T2T2	54	11	7	2
	T3T3	56	10	5	2
	T3T4	40	11	25	5
1.0	T1T4	31	6	11	3
	T2T5	42	9	7	3
	T4T1	25	4	5	1
	T2T6	48	15	10	4
3.0	T1T5	60	10	12	4
	T3T2	-	-	9	3
	T4T2	-	-	11	3
	T4T3	-	-	10	2

Table 3.4: Pond Inlet Pressure Cell Records.

### **3.3 Ice Island Field Program**

In 1987, Mobil Oil Canada Properties, on behalf of the Hibernia Joint Venture Participants, donated the ice indentation system used in Pond Inlet to the Ocean Engineering Research Centre, Memorial University of Newfoundland. Previous tests at Pond Inlet (1984) and in multiyear ice in the Canadian Arctic (1985) had demonstrated the efficiency and the research potential of the system (the multiyear ice data set from 1985 remains proprietary). An experimental program was planned by Memorial University of Newfoundland for the spring of 1989 following intensive refurbishing and additional indenter construction by Geotechnical Resources Arctic Services, now a division of Sandwell-Swan-Wooster Engineering, Calgary, Alberta.

Like previous field indentation experiments, the emphasis of the 1989 Ice Island indentation experiments was data acquisition, primarily intended to investigate recent ice failure theories and improve estimates of design ice pressures and loads. Funding for the program was provided by Transport Canada and Canadian Coast Guard Northern to the level of \$620,000. Research groups, government agencies and industry were involved in the planning of the test series to reflect the interests of all involved in arctic operations.

#### **3.3.1 Equipment Description**

The 1989 Ice Island field program utilized the existing indentation equipment with minimum modifications, but budgetary constraints restricted the system to that of a single actuator. This precluded the use of the large 3.0

m<sup>2</sup> indenter in the proposed testing series. As previously detailed, the indenter system consists essentially of one or more hydraulic actuators mounted upon a mobile skid. The hydraulic system, data acquisition system and test procedures were essentially the same as the Pond Inlet experiments. For the single actuator system, an indenter of specified size, shape, and stiffness would be mounted to the front of the actuator and a fiat back plate attached to the rear. Based on the specifications of the project team, three separate indenters were utilized in the field program:

1. 0.8 m<sup>2</sup> spherical indenter: developed from the existing 1.0 m<sup>2</sup>, 1.28 m radius of curvature, aluminum indenter by reducing the diameter to 1.0 m. The size reduction was necessary to compensate for the reduced power of the single actuator system and to limit the possibility of excessive eccentric loading.
2. 0.8 m<sup>2</sup> circular, flat, compliant indenter: newly constructed based on Canadian Coast Guard Northern formulae for the impact face thickness of ship hull plate. This icebreaker hull simulation was designed to investigate the pressure distribution behind the contact zone and possible "bridging effects" resulting from non-continuous support of the indenter face.
3. 0.375 m<sup>2</sup> rectangular, flat, rigid indenter: pre-existing with dimensions of 500 mm x 750 mm. No reconditioning was required for this indenter, commonly referred to as Meganewt. Extrusion tests on crushed ice performed by Geotechnical Resources Limited and Memorial University

Instrument	Indenter Type		
	Spherical	Flexible	MegaNewt
Load cell	3	3	4
Pressure cell	1	1	4
Displacement pot	1	1	1

Table 3.5: Ice Island Indenter Instrumentation.

of Newfoundland made use of this indenter as well.

A summary of indenter instrumentation for the Ice Island test series is presented in Table 3.5. The spherical indenter was supplied with 100 mm diameter pressure cells, while the flat indenters utilized much smaller (12.7 mm diameter) cells. The layout of the cells for each indenter, illustrated in Figure 3.6, was selected for investigation of the pressure regime across the indenter face.

### 3.3.2 Site Selection

Site selection for the medium scale tests was based primarily on the availability of large quantities of ice and the degree of logistic support that could be procured for that site. With the involvement of Transport Canada and Canadian Coast Guard Northern in the project, it was decided that multi-year ice would be better suited to the testing program (multiyear ice floes and ridges present one of the greatest hazards to arctic shipping). A preliminary survey was conducted and the following identified as potential sites for the field program (see Figure 3.7).

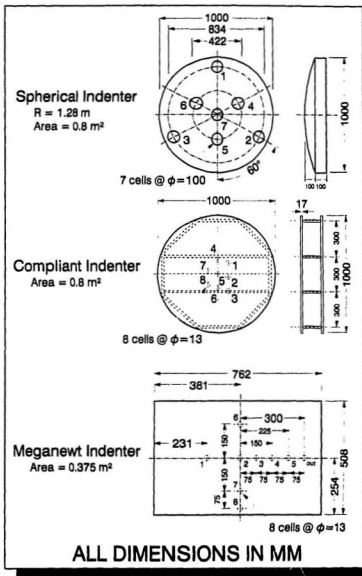


Figure 3.6: Ice Island (1989) Indenter Geometry and Layout of the Pressure Cells.

1. Hobson's Choice Ice Island: a 2.5 kilometer wide, 8.0 kilometer long, 45 meter thick floating block of ice that broke away from the Ward Hunt Ice Shelf, northern Ellesmere Island, in 1982. For the proposed season, the Ice Island was situated northwest of Ellef Ringnes Island at approximately 80° N, 120° W.
2. Eureka, Ellesmere Island: historically, an area with the potential for both iceberg and multiyear ice.
3. Mould Bay, Prince Patrick Island: a region with consistently thick multiyear ice nearby.

Availability of multiyear ice and iceberg-like ice (in the form of freshwater shelf ice) was assured at Hobson's Choice Ice Island but not at the other potential sites. The offices of the Ice Climatology Division of Environment Canada, Ottawa, were visited in early 1989 to assess the ice conditions for Eureka and Mould Bay. Multiyear ice was not forecast for Eureka for the proposed testing period of March-April, 1989. Ice conditions were favourable near Mould Bay, but at a considerable distance away from the base camp. Attention therefore turned to the Ice Island as a potential test site.

Although Hobson's Choice Ice Island is primarily composed of freshwater shelf ice, significant amounts of thick (up to 10 meters) multiyear ice are attached to the shelf ice core. Since 1985, the Polar Continental Shelf Project of Energy, Mines and Resources Canada, or "Polar Shelf", has maintained a base camp on the Ice Island. Scientific expeditions to the Ice Island are coor-



Figure 3.7: Test Location and Other Relevant Centres for the 1989 Ice Island Indentation Test Program.

minated through the Polar Shelf base in Resolute, Northwest Territories, and extensive logistical support is made available to research parties, including accommodations, meals, air travel arrangements, and use of heavy equipment (snowmobiles, bulldozers, etc). With the involvement of Polar Shelf, it was evident that the Ice Island offered the best combination of ice availability and logistical support.

Travel and accommodation of field personnel were quickly and easily arranged through Polar Shelf in Resolute. The indenter was to be shipped to the Ice Island via Resolute on several Hercules C138 flights, though avail-

ability of Hercules aircraft for the proposed testing period was limited and scheduling was critical. A special airstrip also had to be constructed on the island to accommodate the Hercules aircraft. Polar Shelf agreed to provide the airstrip at no cost to the project and work began in early March of 1989. Personnel from Sandwell-Swan-Wooster travelled to the Ice Island in advance of the indenter to prepare a test site and aid in preparation of the airstrip. Ground drifting kept the airstrip snowed in for several days and the Hercules flights were postponed pending snowclearing operations and suitable weather conditions. The indenter and supporting equipment was eventually transported to the island by two Hercules flights on April 9, 1989. Site preparation and system assembly commenced immediately, as well as thorough checks on the computer data acquisition system.

The original test plan foresaw the arrival of most research personnel just prior to the first indentation test. The delays caused by weather conditions and snowclearing operations warranted re-scheduling of travel arrangements for these personnel, but this proved impossible. The limited number of commercial flights to Resolute and the difficulty in changing reservations on short notice saw most research personnel onsite several days before the arrival of the indenter. This additional manpower was put to use in refining the test plan, ice characterization, and restocking the Ice Island fuel dump.

### **3.3.3 Test Preparation**

Indentation experiments were planned in multiyear near the edge of the ice island with the possibility of some additional experiments in the central fresh-

water ice core. Excavation of a long trench some 4 meters deep in the multiyear ice was of priority and proved to be the most time consuming and labour intensive operation of the project. A single trench was favoured on the notion that the indenter system could be lowered into one end of the trench and, following a test, towed a short distance along the trench to the next test face.

A suitable test site in multiyear ice was located about one kilometer southeast of the base camp, cleared of snow and levelled with a bulldozer prior to the arrival of the indenter and supporting equipment. A large heated tent was erected at the test site to allow preparation of the indenter and other equipment in a sheltered, comfortable environment. A smaller heated data acquisition tent was placed on skids for ease of movement as the tests progressed along the length of the trench. A heated enclosure was also constructed for the accumulator skid. Location of the site and other features of the Ice Island are illustrated in Figure 3.8.

Numerous ice cores were taken on the proposed testing site and temperature measurements indicated a projected ice thickness of approximately 10 to 11 meters, leaving 6 to 7 meters of ice below the final projected depth of the trench. A modified "Ditch Witch" trenching unit was utilized to cut two parallel slots 1.5 meters deep, 100 meters long, and 4 meters apart. The area between these slots was raked with a rack of ice ripping tongs attached to the back of a bulldozer, and the broken ice pieces removed from the trench with a small front-end loader. At a depth of approximately 1.2 meters, slots

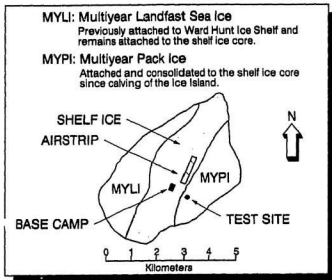


Figure 3.8: Schematic of Hobson's Choice Ice Island (1989)

for the second lift of the trench were cut by the Ditch Witch and chain saws, followed by further ripping and clearing. The 100 meter long trench was excavated to an average depth of approximately 4 meters in 5 days. Plans for a smaller test series in the freshwater shelf ice were put on hold due to time and labour constraints.

Trench walls were roughly squared and smoothed with chain saws and ice chisels. Specific test areas were outlined on the walls in regions free from cracking and those areas were machined to a very smooth finish with a vertically mounted circular saw. The wall opposite the test face was also machined and parallelism of the two faces ensured. Due to the limited load capacity of the single actuator system, it was necessary to shape the impact

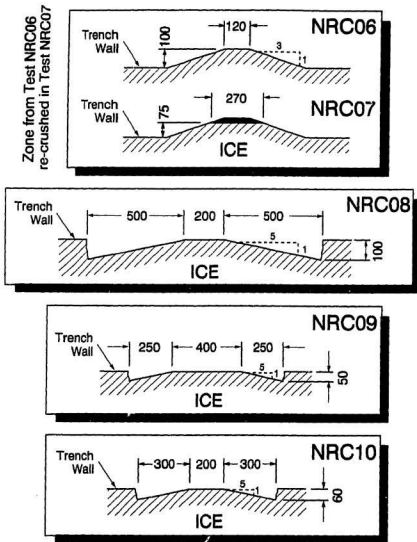
ice face for the flat indenter tests (see Figure 3.9). Failure by crushing and a progressive rise in load with increasing contact area were then achieved.

### 3.3.4 Test Plan

The following were recognized as areas of primary research interest in the indentation test program:

1. **Velocity of Impact:** constant velocities from 1 mm/s to 100 mm/s were adopted to explore rate effects and the transition from brittle to ductile failure.
2. **Indenter Size and Local Structural Stiffness:** indenters of varying size (up to 0.8 m<sup>2</sup>) and stiffness characteristics employed, together with small pressure sensors, to investigate local ice pressure variations.
3. **Characterization of Ice and Failure Zone:** including crushed ice layer and damage zone thickness, failure modes, crack densities, sieve analysis, video records, and ice physical properties.

Based on the requirements of the participants and the primary research interests noted above, the test matrix of Table 3.6 was developed. This matrix has been updated to reflect the actual indenter velocities obtained in the field. The testing procedure for the Ice Island test series was essentially the same as that followed in the Pond Inlet experiments. As the system had not been utilized since 1985, there were some start-up problems and minor delays in the field. A feedback problem delayed the testing by several days but once rectified, testing proceeded as planned.



**ALL DIMENSIONS IN MM**

Figure 3.9: Shaped Multiyear Ice Trench Walls (in Plan) Required for Ice Island Field Program (1989).

Test Number	Test I.D.	Indenter Type	Velocity (mm/s)	Ice Wall Shape
1	ABC01	spherical	0.24	flat
2	NRC01		2.5	flat
3	NRC02		120	flat
4.1	NRC03		6.5	flat
4.2	NRC04		17	flat
5	NRC05		9	flat
6	NRC06	flexible	19.3	1:3 slope
7	NRC07		78.9	1:3 slope
8	NRC08	meganewt	76.9	1:5 slope
9	NRC09		10	1:5 slope
10	NRC10		36.7	1:5 slope

Table 3.6: Test Matrix: Ice Island Indentation Program (1989).

### 3.3.5 Main Results

Like the Pond Inlet experiments, the volume of data collected during the Ice Island field program is immense. Again, only the major findings and some general features of the data set will be presented in this section. Complete load-time data traces are included as Appendix B for those tests which exhibited dynamic activity.

As observed in the Pond Inlet experiments, the Ice Island indentation tests exhibited regular dynamic (sawtooth) behaviour, particularly in the high-speed tests. Several examples of the load-time records are presented in Figure 3.10 and have vibration frequencies on the order of 20 Hz to 40 Hz. Of particular interest in the Ice Island data set was the pressure variation across

the face of the indenter during the test. Numerous small pressure cells were incorporated into the indenter plate for this purpose. The results indicate that local pressures may be as high as 80 MPa and are highly variable across the indenter face, i.e., a simple pressure distribution or one of consistent pattern is not evident for the entire impact zone.

The use of a single actuator in the Ice Island experiments raises questions on the degree of eccentric loading in the tests. Considerable care was taken to ensure proper alignment of the indenter in the trench and parallelism of the trench walls. Still, lateral movement of the indenter was observed in several tests, most likely the result of spalling near the edge of the impact zone. As well, target velocities were not always achieved due to stalling of the single actuator system.

### 3.6 Ultrasonic Measurements

The variation of crushed ice layer thickness with time and the actual thickness of the layer during indentation are very important in ice-structure interaction. In an attempt to acquire data on these variations, the Ice Island experiments utilized an ultrasonic measurement system on a trial basis. The original conceptualization is illustrated in Figure 3.11. The ultrasound probe, with transmitter and receiver in a single unit, was placed in a small borehole at a level equal to that of the center of the indenter. Ethylene glycol would act as a coupling agent between the probe and the ice. The borehole had to be positioned far enough back so the probe would not be damaged by the advancing indenter. Theoretically, the ultrasonic pulses would be reflected

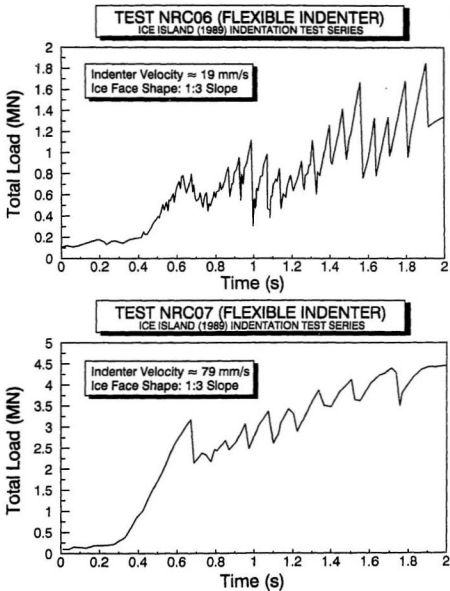


Figure 3.10: Typical Load-Time Records for Hobson's Choice Ice Island (1989) Indentation Test Program.

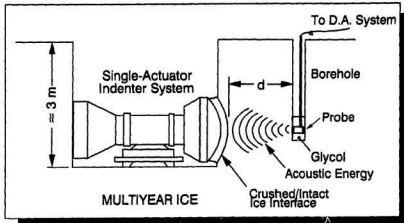


Figure 3.11: Conceptual Arrangement for Ultrasonic Detection of Crushed Ice and Intact Ice Interface, Ice Island (1989).

back to the probe by the interface existing between the highly damaged ice layer near the indenter and the intact ice further back. The distance from the probe to the near surface of the crushed zone would then be known in time. With the movement of the indenter relative to the probe also known, the thickness of the crushed ice layer at any time during the test could be approximated. An idealized situation is illustrated in Figure 3.12.

Initial tests with a portable ultrasound unit were conducted on laboratory grown ice at Memorial University of Newfoundland to establish the feasibility of the proposed measurements. The unit, designed for non-destructive testing of engineering materials, was rented from Eastern Technical Services Limited, St. John's, NF and a representative was present for the lab trials. The

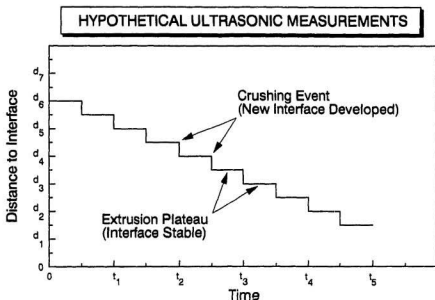


Figure 3.12: Hypothetical Results of Ultrasonic Measurements.

probe was placed in intimate contact with ice blocks of varying thicknesses to determine if the unit could identify the ice-air interface. Overall, the unit performed well, although multiple reflections from cracks and attenuation of the signal by air bubbles occasionally made the output difficult to interpret. It was decided to proceed with the proposed experiments on the Ice Island.

A portable ultrasound unit with a digital output was selected from the stock of NDT Technologies, St. Laurent, P.Q. and the unit picked up in Montréal en route to the Ice Island. When onsite, a set of tests similar to those performed previously at Memorial University confirmed that the unit could identify an ice-air interface. The maximum distance that the ultrasonic pulses could penetrate was a function of the gain, i.e., the lower the frequency,

the greater the penetration distance into the ice mass. As desired penetration distance increased, however, the resolution of the unit decreased, making it difficult to achieve a strong reflection from a small flaw in the material. As the crushed ice layer was expected to be thin, i.e., of the order of 10 mm or less, high resolution was required in order to obtain meaningful results. On the other hand, the probe must be at a safe distance from the indentation zone to prevent damage to the unit. It was clear that a compromise would have to be reached for each test based on the target penetration for that test.

### 3.4 Equipment Performance

When dynamic behaviour was first observed at Pond Inlet, the large variation in load in the sawtooth response was considered significant and steps were taken onsite to isolate the cause. Geotechnical Resources Limited suggested the following as potential mechanisms for the observed dynamic response (Geotech Arctic Services, 1985):

- improper tuning of servo-controller;
- mechanical linkage and system stiffness response; and/or
- progressive ice failure.

Mechanical vibrations are evident in ice-structure interactions where the indenting structure is insufficiently massive or stiff. Resonant vibrations of the structure at one or more of its natural frequencies may compound the problem and create a complex ice failure mechanism. For the indenter

described here, such dynamic behaviour may be expected in cases where the system "feels" rapid large-magnitude drops in load caused by ice failure and cannot compensate quickly enough to maintain the requested displacement profile. The servo-controller utilized at Pond Inlet introduces a constraint in the system which prohibits the actuator from responding to rapid variations in load, i.e., the original displacement profile is preserved. Several checks onsite at Pond Inlet also concluded that observed dynamics were a result of progressive ice failure and subsequent clearing.

## Chapter 4

# Indentation Analysis

The development of a crushed ice layer is the critical stage in the observed dynamic behaviour detailed above. The characteristics of this layer have been studied to some extent in laboratory indentation tests (Kurdyumov and Kheisin, 1976; Jordaan and Timco, 1988), while recent proprietary studies have been undertaken to investigate the behaviour and properties of crushed ice alone. Observations of the crushed ice layer during the Pond Inlet and Ice Island experiments are useful in establishing some general trends in the data sets. Upon withdrawal of the indenter from the test face in the Pond Inlet experiments, a photograph was taken of the crushed ice imprint (Figure 4.1a). This imprint was then sawn into a thin vertical section and a photograph taken of the impact zone profile (Figure 4.1b). A crude scale was drawn on the ice surface and was visible in each photograph.

### 4.1 Crushed Layer Thickness

The size and nature of the ice impact zone are important parameters in ice indentation. Variation in thickness of the crushed ice layer was estimated

**CRUSHED ICE LAYER DEVELOPED BY INDENTATION  
POND INLET (1984) TEST T4T2 (3.0 m<sup>2</sup>)**

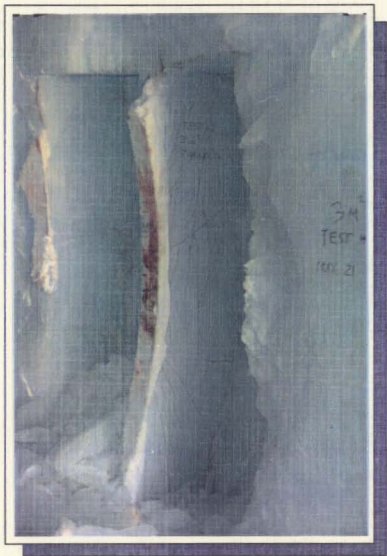


Figure 4.1: (b) Crushed Ice Layer Exposed from a Section Sawn Out of the Pond Inlet (1984) 3.0 m<sup>2</sup> Indentation Imprint (courtesy Mobil Oil Canada Properties).

**CRUSHED ICE LAYER DEVELOPED BY INDENTATION  
POND INLET (1984) TEST T4T2 (3.0 m<sup>2</sup>)**



Figure 4.1: (b) Crushed Ice Layer Exposed from a Section Sawn Out of the Pond Inlet (1984) 3.0 m<sup>2</sup> Indentation Imprint (courtesy Mobil Oil Canada Properties).

for those Pond Inlet tests in which (1) suitable photographs were available and (2) a distinct crushed layer developed. Photographs of the 0.02 m<sup>2</sup> and 0.1 m<sup>2</sup> tests did not clearly show a crushed layer, most likely a result of the very small penetration distance in these tests. The perspective of the crushed layer profile photographs is not known but confidence in the thickness measurements from the photographs is high, since a scale was clearly shown on the profile.

Crushed ice layer profiles from the 1.0 m<sup>2</sup> and 3.0 m<sup>2</sup> tests, abstracted from photographic evidence, are presented in Figure 4.2 and suggest that the shape of the layer varies from test to test. Intuitively, the layer would be expected to be narrowest near the center of the indentation and widest at the edges due to decreasing confinement near the edge of the contact zone. This is very nearly the case in profiles 5 and 6. Other profiles exhibit areas with relatively thick crushed ice layers adjacent to zones with no discernible layer (profiles 2 and 8). It is important to note that the crushed layer profiles presented in Figure 4.2 are representative of the latter stages of the tests, when the indenter was slowing down (recall that the velocity profile in all the Pond Inlet experiments varied from 100 mm/s to zero following a cosine function). Information on the form and variation of crushed ice during all stages of the test would be ideal, but this data is difficult to obtain. Observations of the actual ice/structure interface during the tests are shielded by the indenter itself and compounded by the rapid crushing and ejection of ice from the interface. This adds additional complications to the analysis of an already

**DIGITIZED CRUSHED ICE LAYER THICKNESS PROFILES  
POND INLET (1984) TEST SERIES**

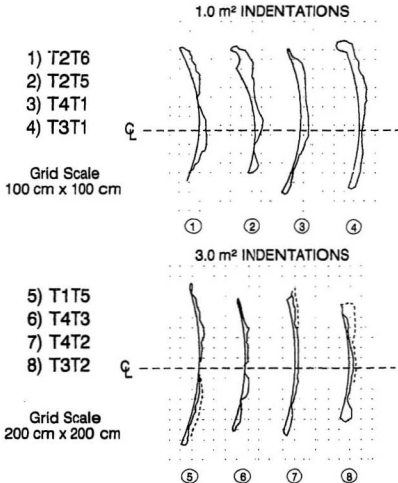


Figure 4.2: Digitized Crushed Ice Layer Thickness Profiles of the Pond Inlet (1984) Indentations. Broken lines indicate zones of damaged, yet relatively intact, ice.

extremely complex interaction.

Table 4.1 presents a set of crushed ice thickness statistics developed for Pond Inlet based on available photographic records. Thickness measurements were taken from the photographs at constant intervals along the indentation profile (the total number of data points depended on the imprint size). In general, mean layer thickness at the end of the test increased with increasing indenter size. It is evident from the statistical range data of Table 4.1 that the thickness of the crushed layer changes and this suggests that crushed ice "patches" or zones develop during the indentations. It is possible to visualize these patches fluctuating across the impact zone depending on local conditions of failure in the area, e.g., non-simultaneous failure in regions with less confinement than other areas. Local pressure variations also suggest that crushed ice patches form and that the crushing and extrusion process is not uniform over the entire face of the indenter.

It is also interesting that a cross-section of crushed ice could be sawn out from the indentation imprint without the crushed layer completely falling away. This suggests that the pulverized material in this region is somewhat solid, the result of a sintering or solidification process under the high impact pressures.

Inlet Size (m <sup>2</sup> )	Test I.D.	Mean Thickness (mm)	Standard Deviation (mm)	Range (mm)
0.5	T2.T1	30	14	50
	T2.T2	9	10	30
	T3.T3	25	9	30
	T3.T4	35	15	50
	All data	25	16	70
1.0	T2.T6	50	20	70
	T4.T1	45	21	60
	T2.T5	55	30	110
	T3.T1	40	21	65
	All data	47	22	110
3.0	T1.T5	75	53	150
	T4.T2	65	20	80
	T4.T3	45	35	100
	T3.T2	80	65	200
	All data	65	42	220

Table 4.1: Crushed Ice Layer Thickness Observations Derived from Photographs of the Pond Inlet (1984) Indentations.

#### 4.1.1 Ultrasonic Measurements

As noted above, details of the form and variation of the crushed ice layer during the complete indentation, rather than only at the end of the test, would be invaluable. For Test NRC-01 of the Ice Island experiments, a trial ultrasonic measurement system was utilized in an attempt to discern the interface between crushed and intact ice. The configuration of the system was previously detailed in Section 3.3.6 and illustrated in Figure 3.11. Based on the programmed command signal for the indentation, the probe was placed in a 50 mm (2") borehole situated 250 mm (10") from the trench wall directly in the path of the 0.8 m<sup>2</sup> spherical indenter. The borehole was filled with the coupling agent (glycol) to approximately 25 mm (1") above the top of the probe. These dimensions represented a compromise between the desired resolution of the measurement (less than 10 mm) and the distance from the trench wall necessary to protect the probe. Output from the probe was fed to the computer data acquisition system via the ultrasound signal conditioner and controller unit. Gain and frequency were adjusted in the data acquisition tent prior to the test and a reflection from the trench wall obtained. Filters were employed to eliminate reflections from flaws, cracks, etc., close to the probe, i.e., to concentrate on the impact zone where the crushed/intact ice interface should develop. Data recording from the ultrasound unit was triggered from the indenter controlling system and is synchronized with all other channels.

Test NRC-01 was mis-programmed and resulted in a very slow indentation

with large stroke. The borehole was breached and the probe extension pole damaged such that the probe could not be extracted for further tests. Results of the ultrasonic measurement system are presented in Figure 4.3. It is difficult to interpret a meaningful trend from such an erratic signal and those areas of interest (spikes) greatly overestimate the distance from probe to indenter. The slow indentation created large cracks in the ice mass around the probe which would act as strong reflectors of the ultrasonic pulse and this may explain the spurious results. Vibrations in the glycol fluid column caused by the advancing indenter would also affect the coupling of the probe to the ice mass.

## 4.2 Sieve Analysis

The degree to which ice is pulverized in high-speed indentations is evident from an analysis of the crushed ice products. During the interactions, crushed ice has been observed to extrude out from behind the advancing indenter and fall away from the indentation zone. For the 1989 Ice Island experiments, crushed ice was collected on a tarpaulin placed on the trench floor below the indenter. Considerable care was taken to ensure that all ice particles ejected from the test surface were recovered. Fines added to the batch by drifting snow and the like were not considered significant. Larger ice fragments caused by brittle spalling were also collected, weighed and photographed.

Significant microcracking near the indenter surface effectively reduces the ice in this region to a mass of particles at the instant of pulverization. As a

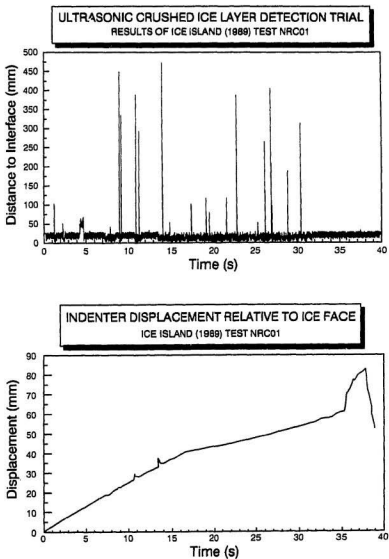


Figure 4.3: Results of the Ultrasonic Crushed Ice Layer Detection Trial, Ice Island (1989) Test Number NRC01.

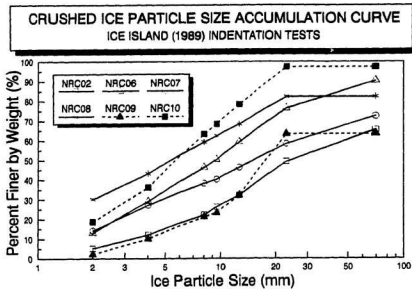


Figure 4.4: Composite Gradation Curve of Crushed Ice Particles from the Ice Island (1989) Indentation Tests.

continuum of discrete particles, crushed ice is sometimes considered a granular material. The sieve analysis is a standard geotechnical engineering technique that lends itself well to crushed ice and was performed during the Ice Island field program to identify the size and distribution of ice particles developed in the interactions. Figure 4.4 is a composite gradation curve for seven indentation tests for which a significant amount of extruded crushed ice was collected. Crushed ice particle size is generally less than 20 mm. The average of the median values ( $D_{50}$ ) for all tests is on the order of 10 mm.

Ice fragments that spalled off the impact zone were also collected for analysis. Spall sizes ranged from small knifelike shards to large blocks weighing over 2 kg. The proportion of spalls was found to be a function of the test

velocity, i.e., the faster the test, the fewer the large spalls. The very large spalling fragments are not representative of the high velocity indentation tests: the production of pulverized ice was more prevalent in these cases.

### 4.3 Spalling and Impact Area Reduction

Spalling of large pieces of ice may reduce the actual contact area during indentation. The presence of large ice fragments in the crushed ice products collected from the Ice Island tests confirms that brittle spalling is an important process in the overall interaction. An idealization of the situation is illustrated in Figure 4.5. Spalling at the edges of the impact zone where confinement is low may reduce the theoretical contact area  $A_t$  to an effective contact area  $A_e$  (which can also include areas of low pressure near the edge of the contact zone). A size effect similar to the idealization of Figure 4.6 may also arise. In an attempt to quantify the degree of spalling, plan photographs of the indenter imprints from the Pond Inlet test series were digitized to determine the actual contact area at the end of the test ( $A_e$ ). The ratio  $A_e/A_t$ , developed for all tests for which suitable photographs were available, gives an indication of the effective reduction in contact area brought on by spalling. The complete data set is presented in Table 4.2. For the 3.0 m<sup>2</sup> tests, for example, final contact areas are on the order of 50% of the theoretical (nominal) value. Size effect based on this data is demonstrated in Figure 4.7.

Utilizing the ratio  $A_e/A_t$  as an area reduction factor for the 1.0 m<sup>2</sup> test (T2T6) yields the average pressure history shown in Figure 4.8. The correla-

Nominal Indenter Area (m <sup>2</sup> )	Theoretical Contact Area A <sub>t</sub> (m <sup>2</sup> )	Test I.D. No.	Digitized Contact Area A <sub>s</sub> (m <sup>2</sup> )	Reduction Factor A <sub>s</sub> /A <sub>t</sub>
0.5	0.51	T3T3	0.22	0.43
		T3T4	0.30	0.59
		Mean	0.26	0.51
1.0	1.03	T1T4	1.06 <sup>†</sup>	1.03
		T2T5	0.67	0.65
		T3T1	0.72	0.70
		T4T1	0.54	0.52
		Mean	0.64	0.62
3.0	3.32	T1T5	2.90 <sup>†</sup>	0.87
		T3T2	1.66	0.50
		T4T2	1.80	0.54
		T4T3	1.59	0.48
		Mean	1.68	0.51

<sup>†</sup> value not used in calculation of the mean.

Table 4.2: Area Reduction by Spalling Derived from Photographs of the Pond Inlet (1984) Indentation Tests.

tion between central pressure and average pressure is particularly good in the circled region, suggesting that, for this region, the crushing/extrusion process occurs near the center of the indenter but over an effective area reduced by spalling.

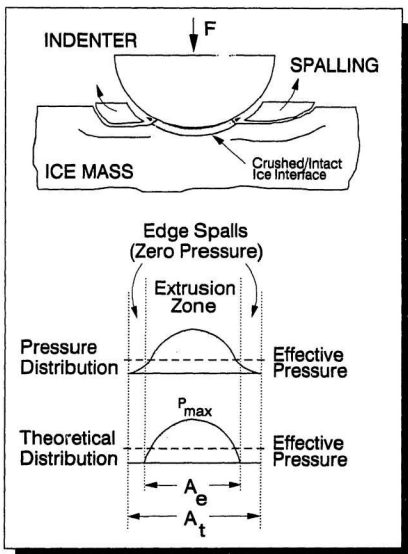


Figure 4.5: Theoretical Reduction of Contact Area by Spalling.

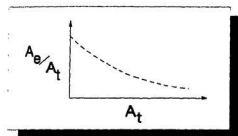


Figure 4.6: Hypothetical Size Effect Resulting from Spalling.

### OBSERVED SIZE EFFECT DUE TO SPALLING POND INLET (1984) TEST SERIES

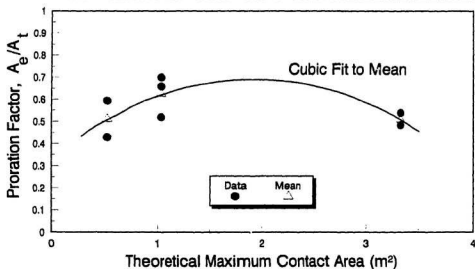


Figure 4.7: Observed Size Effect from Pond Inlet (1984) Data Set.

**CENTRAL PRESSURE AND PRORATED AVERAGE PRESSURE  
POND INLET (1984) TEST T2T6 (1.0 m<sup>2</sup>)**

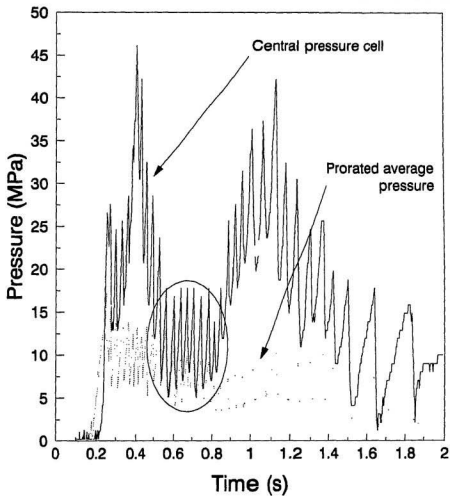


Figure 4.8: Center and Prorated Average Pressure: Pond Inlet (1984) 1.0 m<sup>2</sup>  
Test Number T2T6.

## 4.4 Dynamic Characteristics

Frequency components of load histories for the indentation tests were analyzed by the Fast Fourier Transform (FFT). Each indentation series performed at Pond Inlet (with a particular indenter size) differed in all respects except for the velocity profile, i.e., contact area and penetration distance varied between indenter sizes. For all tests, the initial velocity of the indenter was 100 mm/s and followed a cosine profile to zero. Test length was determined by tailoring this cosine profile to fit the penetration criterion of 10% of the radius of curvature of the indenter ( $0.1R$ ).

For purposes of comparison between individual tests, the indenter velocity profile was adopted as a common feature for the 3.0 m<sup>2</sup> and 1.0 m<sup>2</sup> indentations. Response spectra were developed for five velocity windows during the course of these tests:

1. 100%-95% of initial indenter velocity ( $v_0$ );
2. 95%-85% of  $v_0$ ;
3. 85%-70% of  $v_0$ ;
4. 70%-50% of  $v_0$ ; and
5. 50%-0% of  $v_0$ .

These windows were selected based on the dynamic activity evident during different stages of the test, i.e., dynamic response is more pronounced and of higher frequency in the early stages of the test when indenter velocity is

high. Since vibration frequency decreased as the test progressed, the window length was greater. Note that since the initial velocity of the indenter,  $v_i$ , was 100 mm/s, the percentage values for the windows given above correspond to velocity as well, e.g., 85%-70% is equivalent to 85 mm/s - 70 mm/s. Response spectra for the 0.5 m<sup>2</sup> tests were determined for two windows only. Division of these tests into five velocity windows was impractical due to the short length of the tests (1.41 seconds), i.e., there were insufficient data points in five windows to perform a meaningful spectral analysis.

#### 4.4.1 Test Start-Time

Determination of the test start-time and synchronization of measurements was important to the data analysis. For the analysis of the Pond Inlet experiments presented here, the displacement command signal was checked at an expanded scale and the point at which the signal began to rise fixed as  $t_o=0$ . The data sample number of the command signal trace for this  $t_o$  was noted and applied to the other traces, e.g., if  $t_o$  for the command signal occurred at sample number 506, then  $t_o$  for the load and pressure traces similarly occurred at sample number 506. Illustrated in Figure 4.9, this procedure worked very well and  $t_o$  was determined readily from the command signal and with confidence. The displacement from the test start  $t_o$  until the central load or pressure cell began to sense a response,  $t_c$ , corresponded to the air gap between the indenter and the ice wall prior to the test. A similar synchronization procedure was employed for the Ice Island data set.

EXAMPLE OF METHOD OF DATA TRACE SYNCHRONIZATION

POND INLET (1984) TEST T2T6 (1.0 m<sup>2</sup>)

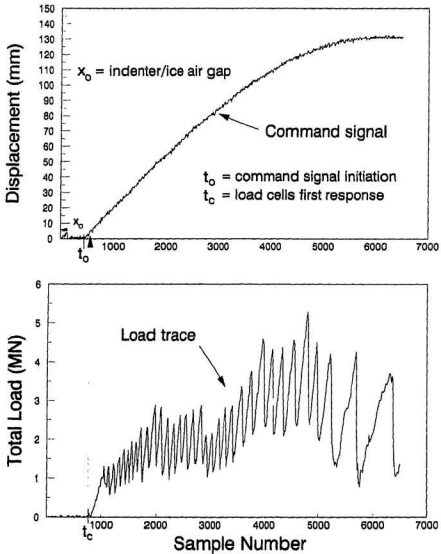


Figure 4.9: Synchronization of Data Traces for Analysis

#### 4.4.2 Response Spectra

Results of the dynamic analysis for the Pond Inlet and Ice Island test series' are presented in Table 4.3. Response spectra were not developed for the Pond Inlet 0.02 m<sup>2</sup> and 0.1 m<sup>2</sup> tests nor the slow Ice Island tests as sawtooth dynamic behaviour was not prominent. One dominant frequency per test (or per window) was observed in the analysis and secondary vibraticn frequencies were not evident. This is clearly illustrated in the examples of the spectral analysis shown in Figure 4.10.

The data of Table 4.3 are presented graphically in Figure 4.11 and indicate that, in general, frequency of vibration decreases with increasing indenter area, but not significantly. Comparison of the 3.0 m<sup>2</sup> and 1.0 m<sup>2</sup> velocity windows suggests that vibration frequency also decreases with decreasing velocity, as expected. In tests T3T2 (3.0 m<sup>2</sup>), T4T3 (3.0 m<sup>2</sup>) and T2T6 (1.0 m<sup>2</sup>), vibration frequency increases following a previous decrease. This would most likely be the result of, for example, non-simultaneous failure or spalling in the early stages of the test followed by the re-establishment of systematic crushing and clearing as contact area increases.

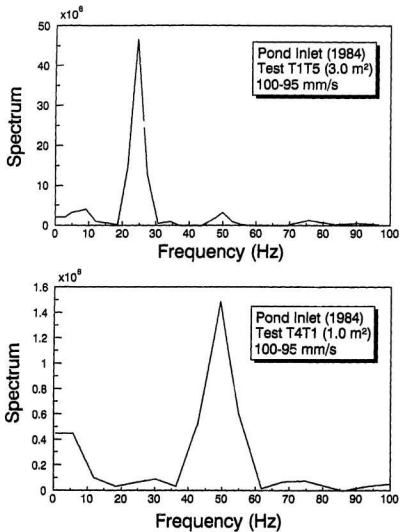
**FREQUENCY RESPONSE SPECTRA OF LOAD**

Figure 4.10: Typical Response Spectra for Medium-Scale Indentation.

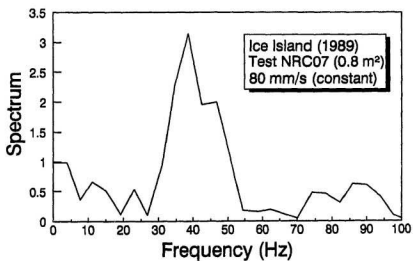
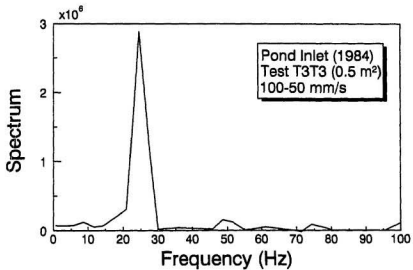
**FREQUENCY RESPONSE SPECTRA OF LOAD**

Figure 4.10: (continued).

Nominal Indenter Area (m <sup>2</sup> )	Test I.D. No.	Velocity Window (% of 100 mm/s)				
		100% to 95% (Hz)	95% to 85% (Hz)	85% to 70% (Hz)	70% to 50% (Hz)	50% to 0% (Hz)
3.0	T1T5	25	16	16	12	7
	T3T2	25	25	32	†	†
	T4T2	25	19	19	13	†
	T4T3	25	19	25	12	7
1.0	T4T1	50	32	32	25	15
	T2T5	25	32	25	18	6
	T2T6	32	25	32	16	6
	T1T4	25	19	15	13	8

Nominal Indenter Area (m <sup>2</sup> )	Test I.D. No.	Velocity Window	
		100% to 50% (Hz)	50% to 0% (Hz)
0.5	T2T1	20	-
	T2T2	10	-
	T3T3	25	10
	T3T4	20	9
0.8 spherical	NRC03		1 <sup>†</sup>
	NRC05		16
0.8 flat	NRC06		14
	NRC07	40	
0.375 flat	NRC08	12	
	NRC10		4 <sup>†</sup>

† end of data file or no dynamics.

‡ two cycles of dynamics only.

Table 4.3: Response Spectra Summary for the Pond Inlet (1984) and Ice Island (1989) Load-Time Records.

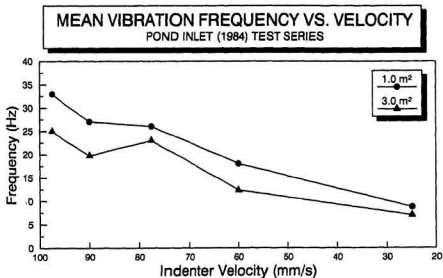


Figure 4.11: Frequency vs. Indenter Velocity for Pond Inlet (1984) 1.0 m<sup>2</sup> and 3.0 m<sup>2</sup> Tests.

## 4.5 Pressure Distributions

The shape and magnitude of the pressure distribution developed behind the indenter are important features of the indentation and provide information on properties of the crushed ice mass. Numerous pressure cells installed at various points along the face of the indenter are required to establish such a distribution. All four indenters used in the Ice Island test program and two of the five Pond Inlet indenters (0.5 m<sup>2</sup> and 3.0 m<sup>2</sup>) were equipped with pressure cells along the indenter surface. Other Pond Inlet indenters were equipped with a single pressure cell at the center of the indenter plate.

In general, local variations in ice pressure during indentation are very high

as compared to the average pressure (computed from total load and contact area). This trend is clear from Table 3.4 of Section 3.2.2 which compares mean and peak pressures for individual pressure cells versus the mean average pressure for all Pond Inlet tests. Local pressures are of importance in the design of structural members and the results of the indentation experiments have implications on current design methodologies. Analysis of the Ice Island data set also indicates that local pressures may fluctuate dramatically across the contact face during the indentation tests.

Local pressure fluctuations suggest that the assumption of a uniform crushed ice layer represents an idealized situation, and that discrete zones or "patches" of thin crushed ice develop. It is postulated that the patches vary in number, location, shape and thickness and develop in areas where conditions for pulverization exist, e.g., zones of very high damage, low confinement or major structural flaws. Tracking the spatial and temporal variations of patch formation would be very difficult, if not impossible. Ultrasound techniques are theoretically promising in this regard, but have not proven feasible under field conditions. Videos taken through a small plexiglass window in a flat, rigid indenter during the 1990 Ice Island program have confirmed the formation of crushed ice patches and the very rapid fluctuations in size, shape and position.

## Chapter 5

### Extrusion Simulation

The behaviour of crushed ice has significant implications for the pressure distributions and total loads arising from medium-scale interactions such as the Pond Inlet and Ice Island experiments. The crushed layer between indenter and intact ice may be modelled from two distinctly different approaches. Pulverized ice particles may be thought of as a granular medium similar to soils, prompting the use of geotechnical techniques, e.g., Hallam and Pickering (1988). Conversely, extrusion of a thin crushed ice layer and the presence of interparticle fluid suggest a flow-based modelling approach, e.g., Kurdyumov and Kheisin (1976). Both approaches are very different in underlying theory, yet both have been shown to have merit in modelling specific features of ice-structure interaction. A consensus has not been reached as to the “best” modelling approach for crushed ice extrusion.

Modelling the entire interaction for the Pond Inlet and Ice Island tests is not attempted here. High-speed ice indentation is an extremely complex process and involves the creation of a new continuum (crushed ice) with prop-

erties uniquely different from the virgin (indented) material. It is impractical to quantify all the parameters involved in the interactions and difficult, if not impossible, to predict the total dynamic response and the occurrence of major events such as spalling. The extrusion cycle has been recognized as one of the most important features of the dynamic behaviour observed in the Pond Inlet and Ice Island indentation programs, and in numerous other laboratory and field observations of ice-induced vibration. Simulation of crushed ice extrusion has therefore been subjected to detailed analysis. Elastic deformations are assumed insignificant, consistent with previous research, e.g., Kurdyumov and Kheisin (1976), and this was confirmed by Xiao (1990) for the case of spherical indentation.

It must be emphasized that the body of data made available by the Pond Inlet and Ice Island field programs is immense and will support further detailed studies for years to come. More than 30 complete indentation tests with high frequency sampling over many channels per test represents a formidable task for any analysis. This data set is compounded further by the fact that up to 40 crushed ice extrusion cycles may be present in a single test. As a result, only typical examples of the analysis are included here.

## 5.1 Spherical Patch Model: Viscous Flow

High local pressures developed in the crushed ice layer during indentation experiments intuitively contradicts the assumptions inherent in Mohr-Coulomb theory. Observations of the crushed ice imprint following the Pond Inlet and Ice Island tests suggest that the layer does not behave like soil or other granular materials. The very fact that a crushed ice imprint remains attached to a vertical test face is convincing evidence that the pulverized ice is a somewhat "solid" material and capable of withstanding load. Some type of sintering mechanism that serves to solidify the crushed material may be at work here. Representation of this crushed ice mass as a viscous fluid has been detailed in the literature and employed in the analysis of small scale indentation experiments. The Pond Inlet and Ice Island data sets afford an opportunity to check the validity of the viscous theory as applied to medium-scale indentations.

The analysis presented here follows the work of Jordaan et al. (1988) for the clearing of crushed ice in fast spherical indentation tests. Indentation of a spherical indenter with radius of curvature  $R$  takes the form of a loaded "patch" of ice, as depicted in Figure 5.1. Crushed ice products develop in a thin layer between the indenter and intact ice and are assumed to extrude outwards from the impact zone along the spherical surface. Crushed ice is treated as a Newtonian incompressible fluid with zero body forces and may be modelled by the Navier-Stokes equations (Schlichting, 1968):

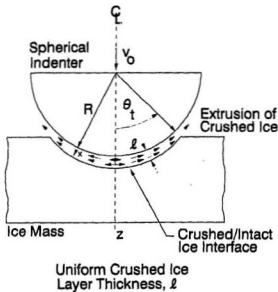


Figure 5.1: Spherical Patch Indentation of an Ice Mass.

$$\rho \frac{d\vec{v}}{dt} + \vec{\nabla} p - \mu \nabla^2 \vec{v} = 0 \quad (5.1)$$

where  $\rho$ : density of crushed ice ( $\text{kg/m}^3$ )

$\vec{v}$ : velocity field (m/s)

$p$ : pressure (MPa)

$\mu$ : dynamic viscosity of crushed ice (kPa·s)

$\vec{\nabla}$ : the gradient vector  $\frac{\partial}{\partial x}(\vec{i}_x) + \frac{\partial}{\partial y}(\vec{i}_y) + \frac{\partial}{\partial z}(\vec{i}_z)$

$\nabla^2$ : Laplacian operator  $\frac{\partial^2}{\partial x^2} + \frac{\partial^2}{\partial y^2} + \frac{\partial^2}{\partial z^2}$

The inertial forces are generally dominated by the viscous forces to the extent that the inertial term in Equation 5.1 may be neglected, yielding:

$$\vec{\nabla} p - \mu \nabla^2 \vec{v} = 0. \quad (5.2)$$

For application to spherical indentation, the reduced Navier-Stokes equations of Equation 5.2 must be transformed from a Cartesian  $(x, y, z)$  to a spherical  $(r, \theta, \phi)$  co-ordinate system. The transformation is very lengthy and incorporates symmetry about the indenter ( $z$ ) axis (M.A. Maes, personal communication). The resulting equilibrium conditions in spherical co-ordinates are as follows:

$$\frac{\partial p}{\partial r} = \mu \left( \nabla^2 v_r - \frac{2v_r}{r^2} - \frac{2}{r^2} \cdot \frac{\partial v_\theta}{\partial \theta} \cdot \frac{2v_\theta \cot(\theta)}{r^2} \right) \quad (5.3)$$

$$\frac{1}{r} \frac{\partial p}{\partial \theta} = \mu \left( \nabla^2 v_\theta + \frac{2}{r^2} \cdot \frac{\partial v_r}{\partial \theta} - \frac{v_\theta}{r^2 \sin^2(\theta)} \right) \quad (5.4)$$

where  $p$ : pressure at coordinates  $(r, \theta)$ ;

$\mu$ : dynamic viscosity;

$v_r$ : radial component of velocity;

$v_\theta$ : tangential component of velocity; and

$\nabla^2$ : Laplacian operator for spherical co-ordinate system.

The Laplacian operator  $\nabla^2$  is given by (Speigel, 1985):

$$\frac{1}{r^2} \frac{\partial}{\partial r} \left( r^2 \frac{\partial}{\partial r} \right) + \frac{1}{r^2 \sin \theta} \cdot \frac{\partial}{\partial \theta} \left( \sin \theta \frac{\partial}{\partial \theta} \right). \quad (5.5)$$

By continuity, the inflow of crushed ice into a small region during indentation must equal the outflow from that region, (Jordaan et al., 1988):

$$\frac{\sin\theta}{r} \cdot \frac{\partial}{\partial r} (r^2 v_r) + \frac{\partial}{\partial \theta} (v_\theta \sin\theta) = 0. \quad (5.6)$$

Equation 5.6 assumes that the dilatation associated with the pulverization process remains constant, i.e., pulverization from loss of shear stiffness is of greater significance than dilatation. A further simplification in the analysis is afforded by lubrication theory, applicable when the layer of crushed ice is relatively thin. This assumption is reasonable in light of the work of, for example, Kurdyumov and Kheisin (1976) and Timco and Jordaan (1988).

Of greater importance in the extrusion process, then, is the variation of tangential velocity,  $v_\theta$ , as a function of  $r$  and the variation of pressure,  $p$ , as a function of  $\theta$ . The Navier-Stokes Equations 5.3 and 5.4 then become:

$$\frac{\partial p}{\partial r} \approx 0 \quad (5.7)$$

$$\frac{\partial p}{\partial \theta} = \frac{\mu}{r} \frac{\partial}{\partial r} \left( r^2 \frac{\partial v_\theta}{\partial r} \right). \quad (5.8)$$

The above simplification renders the continuity equation (Equation 5.6) unsuitable for this analysis, since it has been assumed that  $\frac{\partial v_\theta}{\partial \theta} \approx 0$ . A more suitable equation of continuity was developed by Jordaan et al. (1988) which specifies that "...the volume of crushed ice ejected per unit time through a

circular boundary at an angle  $\theta$  is equal to the volume displaced by the indenter, also per unit time." This leads to:

$$\int_R^{R+\ell(\theta)} v_\theta \cdot 2\pi (r \sin\theta) dr = v_o (\pi R^2 \sin^2\theta) \quad (5.9)$$

where  $\ell(\theta)$ : crushed ice layer thickness; and

$v_o$ : indenter velocity.

Equation 5.8 may be solved by integrating with respect to  $r$ , dividing by  $r^2$ , and integrating with respect to  $r$  once again. Noting that pressure  $p$  is a function of  $\theta$  only, this yields:

$$\mu v_\theta = \left( \frac{r}{2} \frac{dp}{d\theta} \right) - \frac{A(\theta)}{r} + B(\theta). \quad (5.10)$$

The distance  $r$  from the center of the indenter (origin) to a particular point in the crushed ice layer may be expressed as  $r = R + x$ , where  $x$  is the perpendicular distance from that point to the surface of the indenter. In order to solve constants  $A$  and  $B$ , a condition of no-slip is applied at the boundary, i.e.,  $v_\theta = 0$  at both  $x = 0$  and  $x = \ell$ . The solution for  $v_\theta$  becomes:

$$v_\theta = \frac{1}{2\mu} \left( -\frac{dp}{d\theta} \right) \frac{x(\ell - x)}{R} \quad (5.11)$$

which describes a parabolic velocity profile through the crushed layer. Assuming a constant crushed ice layer thickness,  $\ell$ , substitution of Equation 5.11 into the continuity equation (Equation 5.9) yields:

$$\frac{dp}{d\theta} = -\frac{6v_o\mu R^2 \sin\theta}{\ell^3}. \quad (5.12)$$

Recognizing that pressure  $p = 0$  at the edge of the contact zone ( $\theta = \theta_i$ ), integration of Equation 5.12 yields the pressure in the crushed layer as a function of position  $\theta$ :

$$p(\theta) = \frac{6v_o\mu R^2}{\ell^3} (\cos\theta - \cos\theta_i). \quad (5.13)$$

The total load on the indenter is given by:

$$F = \frac{2\pi v_o\mu R^4}{\ell^3} (2 - 3\cos\theta_i + \cos^3\theta_i). \quad (5.14)$$

Equation 5.14, developed by Jordaan et al. (1988), specifies the total load on an indenter during an extrusion cycle of the indentation assuming a viscous crushed ice layer of constant thickness. The authors went on to illustrate the model for the case  $\theta_i = 90^\circ$  (full penetration) based on the results of a 40 mm diameter hemispherical indenter test (Nadreau, 1987).

The Pond Inlet (1984) and Ice Island (1989) experiments utilized spherical indenters with large radii of curvature  $R$  such that  $\theta_i \ll 90^\circ$ . A further simplification of Equation 5.14 is possible in these cases as detailed in Appendix C. The total load on the indenter may therefore be expressed as:

$$F = \frac{3}{2} \frac{\pi v_o\mu R^4 \theta_i^4}{\ell^3}. \quad (5.15)$$

The pressure at the center of the indenter face ( $\theta=0$ ) may be determined from Equation 5.13 as:

$$p_o = 3 \frac{v_o \mu R^2 \theta_i^2}{\ell^3}. \quad (5.16)$$

Equations 5.15 and 5.16 will be applied to the viscous crushed ice extrusion analysis for the Pond Inlet (1984) data set and, to a lesser extent, the Ice Island (1989) test series. Application of the model for the case of constant crushed ice layer thickness is presented in Chapter 6. Parabolic variations in crushed layer thickness may be incorporated into Equations 5.15 and 5.16 but this adds further complications to the simulation of load and pressure from experimental data. Two-dimensional analysis of varying layer thickness is discussed hereafter.

## 5.2 Variable Layer Thickness

Laboratory and field investigations have demonstrated that the thickness of the crushed ice layer is not constant and may vary considerably across the contact zone. For example, medium-scale ice indentation experiments exhibit "hot spots", or small zones where the crushed ice layer may be very thin. This is evident from visual records of the 1984 Pond Inlet test series and local pressure data from the 1989 Ice Island experimental program. In the latter, local pressures across the indenter face fluctuate rapidly and with considerable amplitude, giving the appearance of one or several moving hot spots. This variability can be important in modelling the extrusion process.

### 5.2.1 Incremental Analysis of Irregular Layers

The spherical patch model of Section 5.1 may be extended to incorporate smooth variations in crushed ice layer thickness, but highly irregular layer thickness profiles cannot be modelled in this manner. Consider an arbitrary, irregular, two-dimensional crushed ice layer that has been discretized into numerous segments (Figure 5.2) and in which pulverized ice is ejected from the top and bottom of the contact zone. Extrusion of a single element of the system is analogous to the two-dimensional extrusion of a viscous fluid between two flat parallel plates.

In general, an element of a viscous fluid in motion is subjected to normal, tangential shear, and body forces. The equations of motion for viscous fluid motion, i.e., the Navier-Stokes equations, are developed from a force equilib-

rium on this element. The Navier-Stokes equations for incompressible flow of a constant-viscosity fluid with zero body forces were presented in Section 5.1. Extrusion of a viscous fluid of thickness  $h$  between parallel plates, one of which is advancing at velocity  $v_o$ , is depicted in Figure 5.3 and is described by the two-dimensional form of Equation 5.2:

$$\frac{\partial p}{\partial x} = \mu \cdot \left( \frac{\partial^2 u}{\partial x^2} + \frac{\partial^2 u}{\partial y^2} \right) \quad (5.17)$$

$$\frac{\partial p}{\partial y} = \mu \cdot \left( \frac{\partial^2 v}{\partial x^2} + \frac{\partial^2 v}{\partial y^2} \right). \quad (5.18)$$

The continuity equation for an incompressible fluid is:

$$\frac{\partial u}{\partial x} + \frac{\partial v}{\partial y} = 0 \quad (5.19)$$

where  $u$  and  $v$  are the velocities in the  $x$ - and  $y$ -directions, respectively. At an arbitrary section,  $x_o$ , an average pressure  $\bar{p}$  applies and the mass flow into the segment is described by an average velocity in the  $x$ -direction,  $\bar{u}$ , i.e.:

$$\bar{p} = \left( \frac{1}{h} \right) \int_0^h p(x_o, y) dy \quad (5.20)$$

$$\bar{u} = \left( \frac{1}{h} \right) \int_0^h u(x_o, y) dy. \quad (5.21)$$

The velocity in the  $x$ -direction is assumed zero at the intact ice and indenter interfaces, while the velocity in the  $y$ -direction is assumed to vary from zero

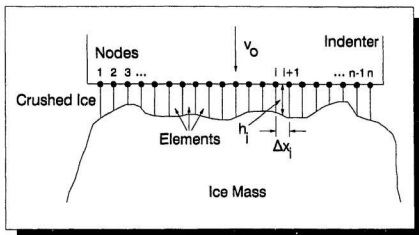


Figure 5.2: Incremental Analysis of Irregular Crushed Ice Layer.

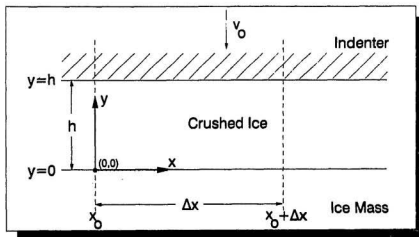


Figure 5.3: Two-Dimensional Extrusion Between Flat Parallel Plates.

at the intact ice interface to  $-v_o$  at the indenter surface. Subject to these boundary conditions, the solution of Equations 5.17-5.19 yields (M.A. Maes, personal communication):

$$u(x, y) = 6\left(\frac{y}{h}\right)\left(1 - \frac{y}{h}\right)\left(\bar{u} + v_o\left[\frac{x - x_o}{h}\right]\right) \quad (5.22)$$

$$v(y) = -v_o\left(\frac{y^2}{h^2}\right)\left[3 - 2\left(\frac{y}{h}\right)\right] \quad (5.23)$$

$$p(x, y) = \bar{p} + \frac{\mu}{h}\left\{v_o\left[6\left(\frac{y^2}{h^2}\right) - 6\left(\frac{y}{h}\right) + 1\right] - 12\bar{u}\left[\frac{x - x_o}{h}\right] - 6v_o\left[\frac{(x - x_o)^2}{h^2}\right]\right\} \quad (5.24)$$

where  $h$  is the thickness of the crushed ice layer. The crushed layer illustrated in Figure 5.2 has been discretized into  $n - 1$  elements (corresponding to  $n$  nodes). Utilizing nodal velocities and pressures averaged over the  $y$ -direction, Equation 5.23, which is a function of  $y$  only, is not required and Equations 5.22 and 5.24 become:

$$\bar{u}_{i+1} = \frac{h_i}{h_{i+1}}\bar{u}_i + \frac{\Delta x_i}{h_{i+1}}v_o \quad (5.25)$$

$$\bar{p}_{i+1} = \bar{p}_i - 12\mu\frac{\Delta x_i}{h_i^2}\bar{u}_i - 6\mu v_o\frac{(\Delta x_i)^2}{h_i^3}. \quad (5.26)$$

For each node  $i=1, \dots, n-1$ , Equations 5.25 and 5.26 apply, yielding a total of  $2(n-1)$  equations for the system. There are  $2n$  unknowns in the system:  $n$  average cross-sectional velocities,  $\bar{u}_i$ , and  $n$  average cross-sectional pressures,

$\bar{p}_i$ . At node numbers 1 and  $n$ , the pulverized ice empties into free space such that  $\bar{p}_1$  and  $\bar{p}_n$  are zero, leaving a total of  $2(n-1)$  variables in the system. The simultaneous Equations 5.25 and 5.26 are then readily solved numerically. The accuracy of this approximation will increase as the number of nodes and constituent elements increases. If the number of elements is large, the average nodal pressure  $\bar{p}_i$  provides a reasonable approximation of the pressure profile across the contact length. Incremental analysis as applied to the results of the Ice Island (1989) data set is discussed in Chapter 6.

### 5.3 Three-Dimensional Extrusion

The spherical patch viscous model of Section 5.1 assumes that crushed ice is extruded through a channel bounded by the indenter and intact ice over the entire indentation area. This approach has been refined by M.A. Maes (Queen's University) such that hot spots can be represented by elliptical patches of varying size and shape and with a variety of crushed ice layer thickness profiles (see Jordaan et al., 1990). Assuming that layer thickness varies quadratically from the center of the hot spot, the zone is then represented by a three-dimensional elliptic paraboloid. Theoretical development of this elegant model is complex and is not presented here, but follows closely the arguments presented in Section 5.1.

For simplicity, the case of incompressibility (constant density) and Newtonian viscous behaviour (constant viscosity) will be adopted, with pressures outside the hot spot assumed zero. In polar coordinates, the solution ob-

tained for the pressure distribution at the hot spot and the total force is as follows (Jordaan et al., 1990):

$$p = \frac{v_o K \mu b^2}{4h_o^3(2 - e^2)} \cdot \left\{ \frac{(2 + \gamma + \gamma(R^2/b^2)) \cdot (1 - (R^2/b^2))}{(1 + \gamma(R^2/b^2))^2 \cdot (1 + \gamma)^2} \right\} \quad (5.27)$$

$$F = \frac{\pi v_o K \mu b^4}{4h_o^3(2 - e^2) \cdot (1 + \gamma)^2 \cdot (1 - e^2)^{\frac{1}{2}}} \quad (5.28)$$

where  $p$ : pressure at point  $(r, \theta)$ ;

$F$ : total force associated with hot spot;

$R$ :  $r^2(1 - e^2 \cos^2(\theta))$ ;

$\mu$ : dynamic viscosity (Pa · s);

$v_o$ : indenter velocity;

$b$ : one-half ellipse minor axis length (2b);

$e$ : ellipse eccentricity =  $(1 - \frac{b^2}{a^2})^{\frac{1}{2}}$ ;

$a$ : one-half ellipse major axis length (2a);

$K$ : velocity profile constant (= 12 for no-slip);

$h_o$ : layer thickness at center of ellipse; and

$\gamma$ : crushed ice layer profile parameter.

Crushed ice layer profile parameter,  $\gamma$ , specifies the shape of the crushed ice thickness profile, e.g.,  $\gamma=0$  corresponds to a constant layer thickness, while  $\gamma=1$  specifies a layer thickness at the edge of the contact zone twice that of

the center.

Elliptical hot spots may vary not only in size and shape but also spatially and temporally. All these variations are important to the interaction as a whole and the resultant pressure distribution and load values. For design purposes, spatial and temporal variations should be incorporated in the model from a statistical standpoint, one that describes the size, shape, thickness, and position of hot spots and the frequency at which they form. Specification of such parameters will clearly require considerable research effort.

## Chapter 6

# Simulation Results and Discussion

Results of the crushed ice layer simulation models detailed in the previous chapter are presented hereafter. Due to the large volume of data available, it was impractical to apply each model to every extrusion curve (upwards of 450 extrusion cycles for both load and pressure). The intention was the assessment of the viscous models as applied to medium-scale ice indentation. The spherical patch model was investigated in greater detail and from the results of numerous simulations, a body of results on layer thickness, viscosity, and contact area was developed for a 1.0 m<sup>2</sup> indentation test. Due to the large number and wide variation of variables involved in the models, simulation of the load and pressure traces required considerable effort. Unfortunately, experimental observations of such critical parameters as crushed ice layer thickness, actual contact area, and crushed ice viscosity were not available. Obtaining meaningful simulations therefore involved specification of these parameters based on past research and informed assumptions.

## 6.1 Spherical Patch Loading

Results from the 0.5 m<sup>2</sup>, 1.0 m<sup>2</sup> and 3.0 m<sup>2</sup> Pond Inlet indentation tests are used exclusively in the following assessment of the patch load model. High indenter velocities were not achieved in the five spherical indentation tests performed in the 1989 Ice Island series and the dynamics, where evident, were short-lived.

For spherical indenters with large radius of curvature, the theoretical total load on the indenter and the center pressure was found to be (Equations 5.15 and 5.16):

$$F = \frac{3}{2} \frac{\pi v_o \mu R^4 \theta_i^4}{\ell^3} \quad (6.1)$$

$$p_o = 3 \frac{v_o \mu R^2 \theta_i^2}{\ell^3}. \quad (6.2)$$

Indenter velocity ( $v_o$ ), radius of curvature ( $R$ ), and indentation angle ( $\theta_i$ ) were known quantities at any stage of a particular test, although indentation angle  $\theta_i$  may be affected by spalling. Quantifying layer thickness ( $\ell$ ) and crushed ice viscosity ( $\mu$ ) was not as straightforward.

### 6.1.1 Layer Thickness Estimates

Information on the thickness profile of the crushed ice layer is available only at the end of the indentation: details of the thickness variations of the layer during the earlier stages of the test must be inferred. This is particularly

true of the Pond Inlet experiments, where the crushed ice profile observed at the end of the test corresponds to that stage where the indenter velocity was near zero. Attempts to discern crushed layer development with ultrasound were not successful. Since the load and pressure predicted by Equations 5.15 and 5.16 are very sensitive to layer thickness ( $\ell^3$ ), good estimates of  $\ell$  are important to the overall simulation.

For example, a portion of the load-displacement curve for Pond Inlet test T2T6 is illustrated in Figure 6.1. Extrusion of crushed ice takes place over a distance of approximately 3 mm, i.e., the crushed ice layer is reduced from an initial thickness ( $\ell_0$ ) mm to  $(\ell_0-3)$  mm. New zones pulverize before the layer thickness is reduced to zero (load is transmitted through the crushed ice products). Extrusion therefore takes place over some fraction of the total crushed ice layer thickness, i.e., layer thickness is somewhat greater than the extrusion distance.

Crushed layer thickness data obtained from digitized photographs of the indentation zone were previously presented in Table 4.1 of Section 4.1. Mean values of layer thickness for the 0.5 m<sup>2</sup>, 1.0 m<sup>2</sup> and 3.0 m<sup>2</sup> tests were 25 mm, 47 mm and 65 mm, respectively. Again, these data represent final values of layer thickness when indenter velocity was near zero. Fine-tuning of  $\ell$  between the observed extrusion distance and final observed layer thickness was reasonable given the otherwise limited knowledge of crushed ice layer thickness.

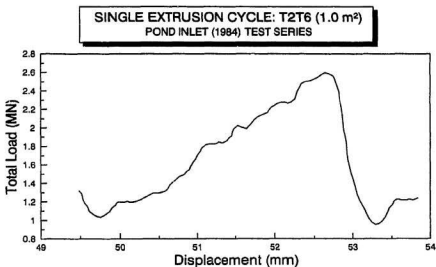


Figure 6.1: Section of Load-Displacement Trace: Pond Inlet T2T6 (1.0 m<sup>2</sup>).

### 6.1.2 Crushed Ice Viscosity

Results of several recent studies on the flow of crushed ice are proprietary and additional research is needed to quantify the viscosity of crushed ice during extrusion. Previous investigators have specified crushed ice viscosities of 10 - 100 kPa-s (Kurdyumov and Kheisin, 1976), 100 kPa-s (Jordaan and Timco, 1988), and 450 kPa-s (Jordaan et al., 1988). These results applied to experiments that may be considered small-scale as compared to the indenter tests described here. It may be inappropriate to adopt a single value of viscosity for all stages of all tests. Indenter velocity will affect viscosity of the crushed layer, but it is difficult to extract this rate effect from other

effects such as increasing confinement.

Figure 6.2 illustrates the effect of crushed ice layer thickness,  $\ell$ , and viscosity,  $\mu$ , on the load predicted by the spherical patch model (all other variables in Equation 5.15 were held constant as shown). For a given load level, several combinations of layer thickness and viscosity satisfy the simulation. For example, at 2 MN load an  $(\ell, \mu)$  combination of (12 mm, 25 kPa·s) or (20 mm, 100 kPa·s) satisfies Equation 5.15. It is difficult to state with certainty that one particular layer thickness/viscosity combination is "correct", given the wide range of possible combinations. Simulation therefore involved fitting the model to experimental data based on reasonable values of  $\ell$  and  $\mu$ . This process was further complicated by variations in contact area during indentation.

### 6.1.3 Contact Area Reduction

Reduction factors for contact area were developed from digitized ice impact zone photographs and suggest that contact area during spherical indentation was less than the theoretical value. Initial simulation runs using the theoretical contact area also resulted in over-estimation of total load for realistic values of viscosity and layer thickness. Variations in contact area became an additional variable in the simulation routines and was initially based on the results of the spalling analysis presented in Section 4.3. The edges of the contact area may also represent zones of very low or near-zero pressures.

Simulations were run utilizing the contact area reduction factors pre-

**SENSITIVITY OF LOAD TO LAYER THICKNESS**  
**CIRCULAR PATCH LOADING MODEL**

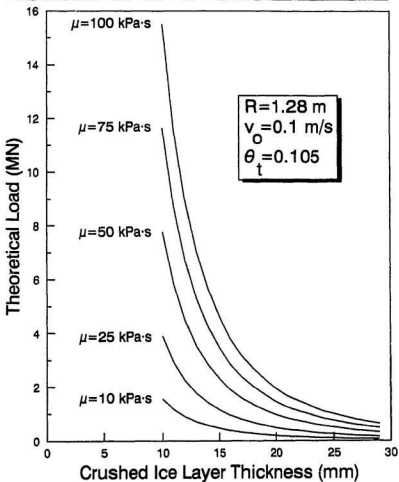


Figure 6.2: Sensitivity of Load vs. Crushed Ice Layer Thickness to Crushed Ice Viscosity.

sented in Table 4.2 of Section 4.3. Simulation of both load and center pressure was impossible for these contact areas due to the sensitivity of the models to contact area (represented by the  $\theta_i$  term in Equations 5.15 and 5.16). The effect is illustrated graphically in Figures 6.3 and 6.4. Since contact area is manifested through  $\theta_i^1$  in the load simulation and through  $\theta_i^2$  in the center pressure simulation, changes in contact area will affect the simulations to varying degrees. Using contact areas specified in the spalling analysis results in theoretical load levels near zero for corresponding pressure levels. It became evident that the area reduction factors taken from the spalling analysis were too low.

### 6.1.4 Simulation Results

Simulation of both load and center pressure simultaneously therefore required optimization of:

1. crushed layer thickness,  $\ell$ ,
2. crushed ice viscosity,  $\mu$ , and
3. contact area (through indentation angle  $\theta_i$ ),

all of which were essentially unknown and for which several combinations of  $\ell$ ,  $\mu$  and  $\theta_i$  may satisfy the model. Sensitivity curves such as those presented in Figures 6.3 and 6.4 were used to establish values of  $\ell$ ,  $\mu$  and  $\theta_i$  within the limits specified by this and previous research. Further experimental work aimed at evaluating these parameters would be a tremendous advantage in

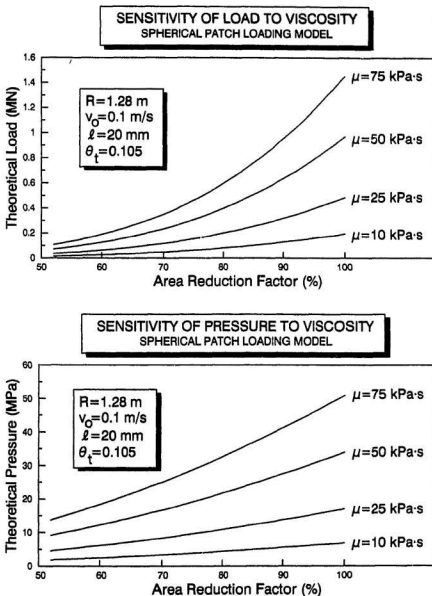
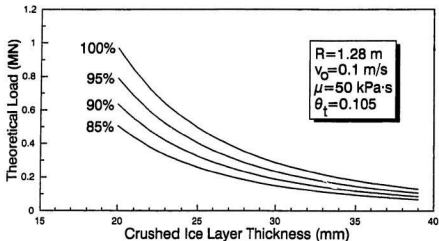


Figure 6.3: Sensitivity of Load and Pressure vs. Area Reduction to Crushed Ice Viscosity.

**SENSITIVITY OF LOAD TO AREA REDUCTION FACTOR**  
SPHERICAL PATCH LOADING MODEL

104



**SENSITIVITY OF PRESSURE TO AREA REDUCTION FACTOR**  
SPHERICAL PATCH LOADING MODEL

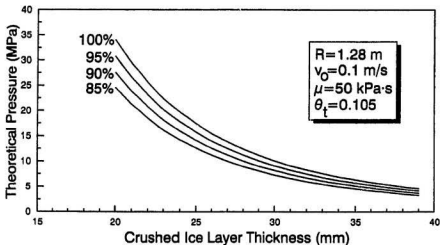


Figure 6.4: Sensitivity of Load and Pressure vs. Crushed Ice Layer Thickness to Area Reduction Factor.

assessing the model.

Examples of simulation results for a single extrusion cycle of the 0.5 m<sup>2</sup> and 1.0 m<sup>2</sup> Pond Inlet indentation experiments are presented in Figures 6.5 and 6.6. In general, load and center pressure predictions from the model compare very well with the experimental data. In order to investigate the range of viscosity ( $\mu$ ), layer thickness ( $\ell$ ) and contact area ( $\theta$ ) for different stages of indentation, a series of simulations were performed for Pond Inlet 1.0 m<sup>2</sup> test T2T6. Of all the tests conducted at Pond Inlet and on the Ice Island, Pond Inlet Test T2T6 exhibited a very regular sawtooth response in both load and center pressure (Figure 6.7). This implied that crushing activity was taking place primarily in the center of the impact zone near the central pressure cell. These results provided an ideal opportunity to assess the spherical patch model.

Each extrusion cycle of the sawtooth curve from T2T6 was isolated and the spherical patch simulation run to determine the combination of  $\mu$ ,  $\ell$  and  $\theta$ , that yielded the optimum fit to the experimental data. A chi-square goodness-of-fit criterion was used to identify the optimum fit for both load and center pressure simultaneously. Determination of the best fit for each extrusion cycle required considerable computer time as three variables were systematically varied over wide ranges.

Results of the analysis are presented in Table 6.1. Layer thickness,  $\ell$  (Column 5), refers to the layer thickness at the start of the extrusion cycle.

## SPHERICAL PATCH LOADING SIMULATION

### POND INLET (1984) TEST T2T1 (0.5 m<sup>2</sup>)

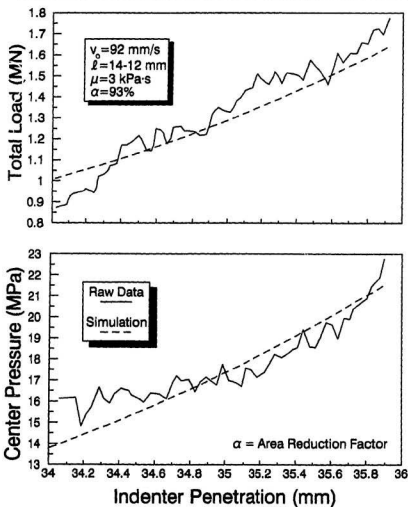


Figure 6.5: Simulation Results (0.5 m<sup>2</sup>): Pond Inlet Test Number T2T1.

**SPHERICAL PATCH LOADING SIMULATION**  
**POND INLET (1984) TEST T2T6 (1.0 m<sup>2</sup>)**

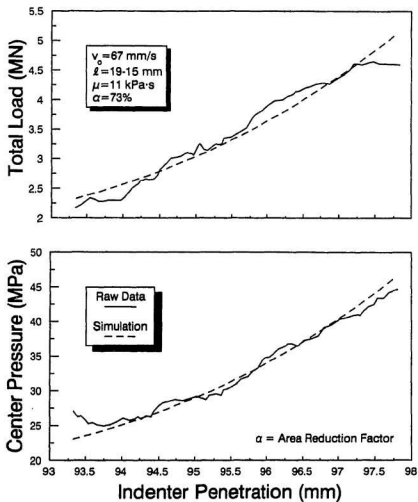


Figure 6.6: Simulation Results (1.0 m<sup>2</sup>): Pond Inlet Test Number T2T6.

**TOTAL LOAD AND CENTRAL PRESSURE RECORDS**  
POND INLET (1984) TEST T2T6 (1.0 m<sup>2</sup>)

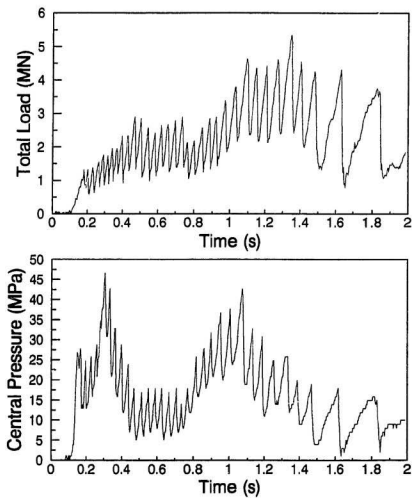


Figure 6.7: Pond Inlet T2T6 (1.0 m<sup>2</sup>): Total Load and Center Pressure Traces.

Layer thickness at the end of the extrusion cycle is equal to  $\ell$  minus the extrusion distance given in Column 2. Table 6.1 has also been divided into five sections corresponding to the velocity windows specified in the dynamic analysis of Section 4.4.

### 6.1.5 Discussion

The spherical patch model simulations presented in Figures 6.5 and 6.6 demonstrate that treatment of crushed ice as a viscous material is an encouraging technique. Indeed, the simulations of load and center pressure are exceptionally good in most cases, particularly for Pond Inlet test T2T6 (1.0 m<sup>2</sup>). Even so, it is important to note that three parameters in the model were varied independently to optimize the fit between experimental data and the simulation results. The simulations therefore do not represent an irrefutable validation of the viscous model, rather a calibration of the model to the experimental data set.

Some general observations can also be made of the simulation data set for T2T6 presented in Table 6.1. Crushed ice viscosity is generally less than 10 kPa·s with a mean of  $\bar{\mu}=4.5$  kPa·s. These figures compare well with the low end of the viscosity range reported by Kurdyumov and Kheisin (1976). Crushed ice layer thicknesses are very reasonable ( $\bar{\ell}=15$  mm) but are consistently less than that determined from the crushed layer profiles described in Section 4.1. This is not surprising given that the profiles represent the situation that exists at the end of the test, when the indenter was slowing

Average Indenter Displacement Over Interval (mm)	Extrusion Distance (mm)	Average Indenter Velocity Over Interval (mm/s)	Simulation Results for Best Fit		
			Viscosity $\mu$ (kPa-s)	Thickness $\ell$ (mm)	Area Reduction Factor
19.0	1.0	98.9	2	9	0.86
21.5	2.1	98.6	2	12	0.91
24.5	2.5	98.2	2	12	0.89
27.5	2.2	97.7	4	14	0.87
30.0	1.7	97.2	8	14	0.78
32.0	1.7	96.8	9	12	0.72
34.5	1.9	96.3	12	15	0.75
37.5	2.1	95.6	7	16	0.82
40.5	2.8	94.8	3	14	0.83
44.0	3.1	93.9	2	16	0.93
47.5	2.5	92.8	5	25	0.98
51.0	2.9	91.7	1	16	0.95
54.5	2.6	90.4	1	15	0.92
58.0	2.8	89.1	1	15	0.92
61.5	2.6	87.7	5	24	0.91
65.0	2.9	86.2	1	16	0.92
68.5	2.6	84.5	1	16	0.92
71.5	1.6	83.0	1	16	0.91
74.0	2.2	81.7	1	13	0.81
77.0	2.8	79.8	1	12	0.79
80.5	2.8	77.8	2	13	0.75
83.5	2.7	75.7	5	16	0.73
87.0	3.4	73.3	9	18	0.71
91.0	3.3	70.2	8	18	0.73
95.5	4.0	66.7	11	19	0.73
99.5	3.0	63.1	5	17	0.77
103.0	3.1	59.5	3	15	0.77
106.5	3.1	55.7	1	13	0.84
110.0	3.5	50.9			
113.5	2.1	46.1	1	12	0.84
116.5	2.6	41.2	15	5	0.50
		Mean	0.0045	15	0.82
		Range	0.014	20	0.48
		Standard Deviation	0.004	4	0.10

Table 6.1: Pond Inlet T2T6: Extrusion Simulation Results.

down.

The average reduction in contact area predicted by the simulations is on the order of 80% as compared to 65% determined from the spalling analysis of the 1.0 m<sup>2</sup>. Crushed ice falling away from the impact zone when the indenter is withdrawn would account for the lower estimate of contact area. In this light, the figure of 80% is more acceptable.

Consider the variation in contact area with respect to indenter velocity for the extrusions detailed in Table 6.1 above. Theoretical contact area during the test is specified by test geometry and other known variables, e.g., indenter displacement profile. A reduced contact area for the test may be computed by applying the area reduction factor (Column 6 of Table 6.1) to the theoretical contact area. Figure 6.8 illustrates the variation in contact area with indenter velocity for the theoretical case and for the results of the spherical patch model. Data points shown are average values of contact area and velocity over the small extrusion intervals. Contact areas predicted by the spherical patch model follow the theoretical limit as indenter penetration increases. In the early stages of the test, computed contact area is essentially equal to the theoretical value. At approximately 80 mm/s, contact area decreases and a greater discrepancy between theoretical and computed area exists. The model continues to follow the general trend of increasing contact area, however, and this is encouraging for the model as a whole.

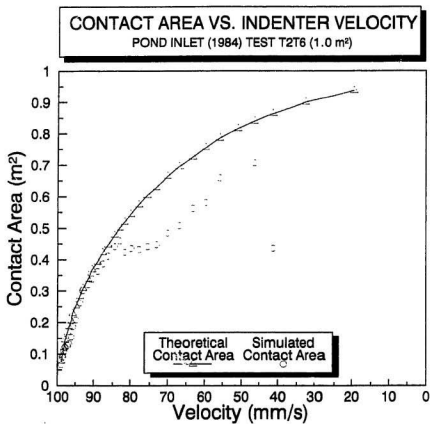


Figure 6.8: Contact Area vs. Indenter Velocity for the Spherical Patch Simulation of Pond Inlet Test Number T2T6 (1.0 m<sup>2</sup>).

## 6.2 Variable Layer Thickness

Some general examples of a two-dimensional incremental analysis are illustrated in Figure 6.9 for a variety of crushed ice layer profiles and a standard contact length of 1 meter. Indenter velocity was fixed at  $v_o = 0.1$  m/s and the viscosity of crushed ice held constant at  $\mu = 50$  kPa·s. A constant layer thickness results in the classical pressure distribution shown in Figure 6.9a, and is also applicable to the spherical patch model results detailed in the previous section. A gradually varying layer thickness profile, thin near the center of the contact length and thicker near the free surface, exhibits a distinct peak in pressure in the thin zone, i.e., representing a “hot spot” (Figure 6.9b). The highly irregular layer example of Figure 6.9c similarly exhibits a pressure peak for a hot spot that has developed near the edge of the contact length. Pressures in these hot spots are considerably higher than the average pressure for the entire contact width, consistent with the observations on the Ice Island and at Pond Inlet.

For illustrative purposes, incremental analysis has been applied to the results of one of the  $0.375 \text{ m}^2$  flat rectangular indenter tests from the 1989 Ice Island test series. Test NRC08 achieved a penetration of 31 mm at a velocity of approximately 80 mm/s. Pressure data which suggested the presence of a hot spot near the center of the indenter were selected for comparison to the simulation routine. Pressure cells numbers 1, 2, 3 and 4, situated horizontally along the centerline of the indenter, were used in the simulation (layout of the pressure cells was previously illustrated in Figure 3.7). To

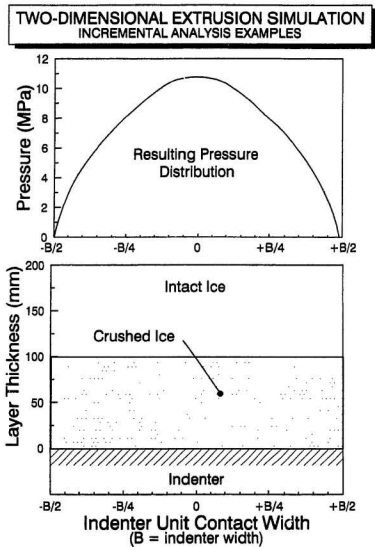


Figure 6.9: (a) Two-Dimensional Incremental Analysis Examples.

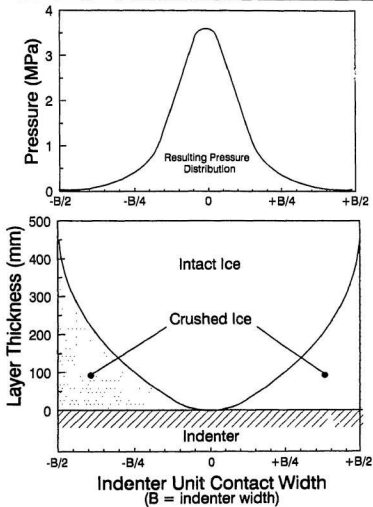
**TWO-DIMENSIONAL EXTRUSION SIMULATION  
INCREMENTAL ANALYSIS EXAMPLES**

Figure 6.9: (b) Two-Dimensional Incremental Analysis Examples (continued).

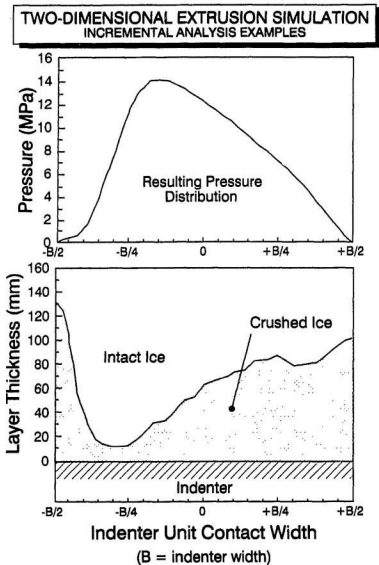


Figure 6.9: (c) Two-Dimensional Incremental Analysis Examples (continued).

investigate the effect on crushed ice layer thickness profiles, contact area and crushed ice viscosity were held constant and various thickness profiles used for comparison. A typical example only is shown here and employs a smooth profile: highly irregular profiles require discretization into many elements, which then requires considerable computer time to solve the set of simultaneous equations.

Data corresponding to a penetration of 25 mm ( $t=3.8$  s) were selected to ensure that the outer pressure cells registered a response. At this penetration, the contact width (based on the geometry of the shaped ice face) was approximately 450 mm. Simulation results are illustrated in Figure 6.10 for a viscosity of  $\mu = 100$  kPa·s and a fifth-order polynomial crushed layer thickness profile.

### 6.2.1 Discussion

The two-dimensional extrusion model is of greatest interest for highly irregular crushed ice layer thickness profiles. Unfortunately, detailed information on the actual variation of layer thickness during an indentation test is not available. It may be possible to estimate a profile by making educated guesses of layer thickness at pressure cell locations. Layer thickness contours could then be drawn through the cells based on the local pressure measurements. This would be extremely time-consuming and a considerable amount of fine-tuning of the thickness profile would be necessary. Further research would be required in order to extend the incremental analysis technique to a more useful form, e.g., three-dimensional irregular layers.

**TWO-DIMENSIONAL EXTRUSION SIMULATION**  
**ICE ISLAND (1989) TEST NRC08**

118

Velocity = 80 mm/s  
Penetration = 25 mm  
Viscosity = 0.10 MPa·s

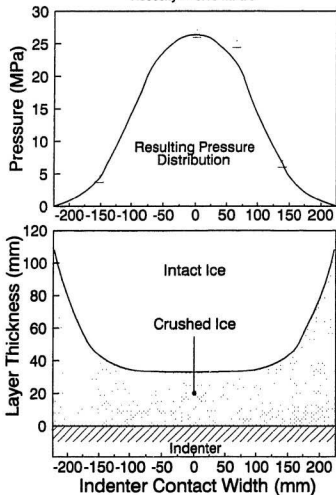


Figure 6.10: Incremental Analysis Simulation Results for Ice Island Test NRC08.

### 6.3 3-D Extrusion

Some examples of the type of pressure distributions predicted by the three-dimensional extrusion model are presented in Figure 6.11 for the cases of (a) constant layer thickness ( $\gamma=0$ ) and (b) edge thickness four times the central thickness ( $\gamma=3$ ). Note how the distribution becomes more peaked as the layer thickness at the edge of the hot spot increases. Peak pressure decreases, however, as  $\gamma$  increases.

An example of the elliptical 3-D extrusion model is presented using data from the Pond Inlet experiments. The first of the Pond Inlet 3.0 m<sup>2</sup> indentation tests (T1T5) included five pressure cells situated in an array as shown in Figure 3.3. The traces from each of these pressure cells are depicted in Figure 6.12. Note the strong peaks from the central pressure cell during the initial stages of the test when the contact area is relatively small. It is impossible to determine exactly the actual extent, shape and position of hot spots during the course of this indentation test. Model simulations are still possible, however.

As an example, consider the pressure regime that occurs at time  $t=1.76$  seconds of Pond Inlet test T1T5. Pressure values for each of the five cells are as follows:

Cell Number	Pressure (MPa)
P1	10
P2	4
P3	2
P4	0
P5	1

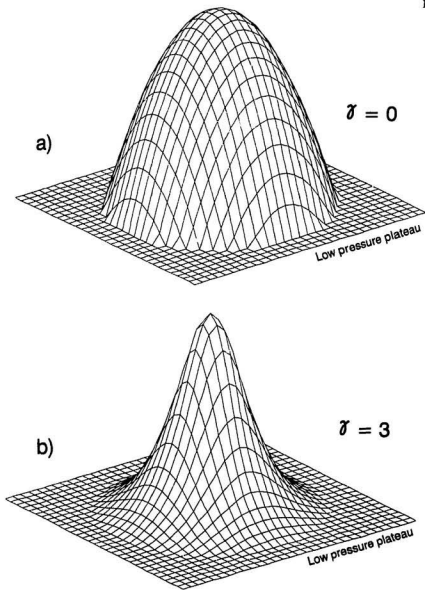


Figure 6.11: Typical Pressure Distributions for 3-D Extrusion Simulation.

The corresponding load at time  $t=1.76$  seconds is  $F=4200$  kN and occurs near the midpoint of the rising part of the force-time curve (see Figure 6.13). Let the hot spot be represented by a circle of radius 600 mm centered at pressure cell P1 (note that a circle is the limiting case of an ellipse with eccentricity  $e=0$ ). The radius of 600 mm was specified by the distance from the center pressure cell to the outermost cell (where the pressure was assumed zero, i.e., the edge of the contact zone). Results of the simulation are illustrated in Figure 6.14 for the input parameters noted on the figure. Layer profile parameter  $\gamma=1$  corresponds to a layer thickness at the extremity of the hot spot of twice the central thickness ( $h_o$ ) with a quadratic variation in between. Pressures from the simulation fit very well with experimental values, particularly the central and outermost cells. Pressure P2 is overestimated. Load also corresponds very well, with the model predicting 4200 kN, the same as the experimental value.

Contact area is very important to the model and greatly affects the total load predicted in the simulation. The hot spot dimension ( $r=0.6$  m) utilized above corresponds to a contact area of approximately  $1.15$  m<sup>2</sup>, whereas the theoretical contact area for  $t=1.76$  seconds is  $2.3$  m<sup>2</sup>. This would suggest that the simulation does not fairly represent actual contact areas developed in the indentation. However, recall that spalling may play a significant role in the interactions, along with areas of low pressure near the edge of the contact zone. From the digitized impact zones, an area reduction factor of 51% was determined. When applied to the theoretical contact area of  $2.30$

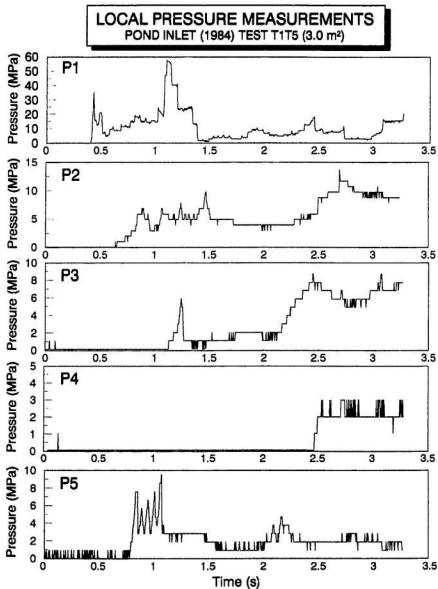


Figure 6.12: Pressure Traces, Pond Inlet 3.0 m<sup>2</sup> Test Number T1T5 for Pressure Cells P1 Through P5.

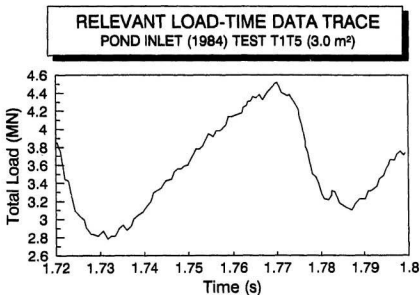


Figure 6.13: Relevant Load-Time Trace, Pond Inlet Test Number T1T5 (3.0 m<sup>2</sup>).

m<sup>2</sup>, the prorated contact area (1.17 m<sup>2</sup>) and that specified by the simulation (1.15 m<sup>2</sup>) are in excellent agreement.

### 6.3.1 Discussion

Unlike the spherical patch model, the 3-D hot spot simulation incorporates different contact zone shapes as well as areas. The limiting cases of the model are essentially the spherical patch model (ellipse eccentricity  $e=0$ ) and the two-dimensional incremental analysis ( $e=1$ ). The example presented above demonstrated the 3-D model for the case  $e=0$ , but this can be extended to hot spots of various elliptical shapes. As is the case with the two-dimensional extrusion model, specification of hot spot formation times, shapes, sizes and locations is a difficult task. Additional testing programs and statistical tech-

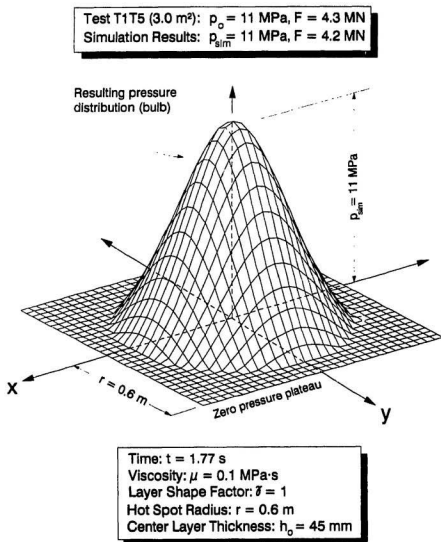


Figure 6.14: 3-D Viscous Extrusion Simulation Results for Pond Inlet Test Number T1T5 (3.0 m<sup>2</sup>).

niques would be required to incorporate all these parameters into the model.

The simulation examples of Figures 6.11 and 6.14 show the pressure distribution, or pressure "bulb", tending to zero at the edge of the hot spot. This may not be the case; rather, the edge of the hot spot may be typified by a transitional zone existing between the high-pressure hot spot and a low-pressure plateau (not necessarily zero pressure). The onset of this transitional zone may mark the point at which the viscous treatment of crushed ice becomes invalid. Crushed ice under low pressure outside this zone may behave as a granular material.

## Chapter 7

# Conclusions and Recommendations

Results of the medium-scale ice indentation experiments at Pond Inlet (1984) and on Hobson's Choice Ice Island (1989) represent one of the largest and most comprehensive data sets available on ice-induced vibration. The experiments were designed to investigate ice-structure interactions under controlled conditions and on a scale larger than standard ice-tank tests. Highly regular dynamic activity was observed as a very important feature of both experimental programs, with vibration frequencies of the order of 30 Hz common. Alternate pulverization of ice and extrusion of the crushed ice products was recognized as the primary mechanism for the observed dynamics. For this investigation, attention was focused on the role that crushed ice plays in the development of the characteristic sawtooth response.

Indentation of ice is an extremely complex process. The interaction of ice and structure results in the destruction of the parent material (intact ice) and the production of a new continuum (crushed ice). The contact zone is

shielded by both the indenter and extruding crushed ice such that observations of contact area, crushed ice zone position and layer thickness are not possible. Information on these parameters is only available *after* a test. In the 1989 Ice Island field program, detection of the crushed/intact ice interface in real time was unsuccessfully attempted with ultrasound techniques. Further research is needed to develop practical methods to monitor the formation and variation of crushed ice zones during indentation. Three-dimensional acoustic emission techniques may prove useful in this regard.

Pulverized ice products possess physical properties quite unlike those of the parent material. How crushed ice behaves during indentation is very important in the simulation of load and pressure. Discrete crushed ice particles have been suggested to behave as a granular (geotechnical) material, but under high indentation pressures, pulverized ice has been observed as a pasty, powder<sup>v</sup> substance. This led to the analogy of crushed ice as a viscous fluid which is squeezed out from between the indenter and intact ice under high pressure. Three models that treat crushed ice as a linear viscous fluid were presented for analysis of the Pond Inlet and Ice Island data set: (1) spherical patch loading with constant crushed ice layer thickness, (2) two-dimensional incremental analysis of irregular crushed ice layer profiles, and (3) three-dimensional extrusion over an elliptical contact zone. All models performed well, although the data set was better suited to the spherical patch model and simulations of load and center pressure.

General conclusions based on the indentation analysis and simulations detailed in this work may be briefly summarized as follows:

1. Memorial University of Newfoundland's medium-scale ice indentation apparatus is a reliable and versatile research system.
2. Alternate pulverization and extrusion of crushed ice is recognized as the primary mechanism for the observed dynamics.
3. During indentation, high local pressures may occur in thin zones of crushed ice (hot spots) within a larger matrix under low or near zero pressure.
4. Simulation of crushed ice as an extruding viscous fluid is an encouraging analysis technique.
5. Based on the results of a series of simulations for a  $1.0 \text{ m}^2$  spherical indentation test, the average viscosity of crushed ice was approximately  $5 \text{ kPa}\cdot\text{s}$ .

Additional information on the spatial and temporal variations of crushed ice during indentation is required for more detailed modelling of the indentation process. Statistical techniques would be useful in that regard. Another important aspect is specification of the peak load or pressure for the extrusion cycle, i.e., at what load or pressure does a new zone of ice pulverize? This will depend on a variety of factors including the local pressure regime, area effects, the flaw distribution in the ice, and the degree of confinement.

## References

- Blenkarn, K.A., 1970. "Measurement and Analysis of Ice Forces on Cook Inlet Structures", **Second Annual Offshore Technology Conference**, April 22-
- Bowles, J.E., 1982. **Foundation Analysis and Design**, McGraw-Hill Book Co., New York, 816 pp.
- Danielwicz, B. and Blanchet, D., 1988. "Measurements of Multi-Year Ice Loads on Hans Island During 1980 and 1981", **POAC '87**, Proceedings of the Ninth International Conference on Port and Ocean Engineering Under Arctic Conditions, Fairbanks, Alaska, Vol. 1, pp. 465-484.
- Danys, J.V., 1977. "Ice Forces on Old and New Offshore Lighthouses in the St. Lawrence Waterway", **POAC '77**, Proceedings of the Fourth International Conference on Port and Ocean Engineering Under Arctic Conditions, St. John's, Newfoundland, 24 pp.
- Dorris, J.F., 1989. "A Plasticity Model for the Crushing of Ice", **IUTAM/IAHR Symposium on Ice Structure Interaction**, August 14-17, St. John's, Newfoundland, Canada (in press)
- Engelbrektsen, A., 1977. "Dynamic Ice Loads on a Lighthouse Structure", **POAC '77**, Proceedings of the Fourth International Conference on Port and Ocean Engineering Under Arctic Conditions, St. John's, Newfoundland, Canada, 10 pp.
- Finn, D.W., Jordaan, I.J., Singh, S.K. and Spencer, P., 1989. **Flow of Crushed Ice: Physical and Mechanical Properties and Behavior**, Ocean Engineering Research Centre, Memorial University of Newfoundland, St. John's, NF (proprietary)
- Geotech Arctic Services, 1985. **Medium Scale Iceberg Impact Simulation Test Program**, prepared for Mobil Oil Canada, Ltd. and the Hibernia Joint Venture Participants, in three volumes
- Glen, I. and Comfort, G., 1983. "Ice Impact Pressure and Load: Investigation by Laboratory Experiments and Ship Trials", **POAC '83**, Proceedings of the Seventh International Conference on Port and Ocean Engineering Under Arctic Conditions, Vol. 1, Helsinki, Technical Research Centre of Finland, VTT Symposium 27, pp. 516-533.
- Gordon, E.W. and Montgomery, C.J., 1981. **Dynamic Response of Bridge Piers to Ice Forces**, Structural Engineering Report No. 96, Department of Civil Engineering, University of Alberta, Edmonton, 222 pp.

- Hallam, S.D. and Pickering, J.G., 1988. "Modelling of Dynamic Ice Loading of Offshore Arctic Structures", **POLARTECH '88**, Proceedings of the International Conference on Technology for Polar Areas, Trondheim, Norway, Vol. 1, pp. 235-248
- Iyer, S.H., 1989. "A State-of-the-Art Review of Local Ice Loads for the Design of Offshore Structures", **IAHR Working Group on Ice Forces 4th State-of-the-Art Report**, CRREL Special Report S9-5, pp. 1-57.
- Janbu, N., Jizu, X. and Grande, L., 1983. "The Collapse of a Flare Jacket Subjected to Ice Loads", **Behaviour of Offshore Structures**, Proceedings of the Third International Conference (ed.'s Chryssostomidis and Connor), Vol. 2, pp. 401-414
- Jefferies, M.G. and Wright, W.H., 1988. "Dynamic Response of "Molikpaq" to Ice-Structure Interaction", **OMAE '88**, Proceedings of the Seventh International Conference on Offshore Mechanics and Arctic Engineering, February 7-12, Houston, Texas, pp. 201-220.
- Jizu, X., 1981. "Dynamic Response of a Jacket Platform Subjected to Ice Loads", **POAC '81**, Proceedings of the Sixth International Conference on Port and Ocean Engineering Under Arctic Conditions, Quebec, Canada, Vol. 1, pp. 503-516.
- Johnson, R.C. and Benoit, J.R., 1987. "Iceberg Impact Strength", **OTC '87**, Proceedings of the 19th Offshore Technology Conference, Houston, Texas, pp. 417-423.
- Jones, S.J., 1982. "The Confined Compressive Strength of Polycrystalline Ice", **Journal of Glaciology**, Vol. 28, No. 98, pp. 171-177.
- Jordaan, I.J. and McKenna, R.F., 1989. "Processes of Deformation and Fracture of Ice in Compression", **IUTAM/IAHR Symposium on Ice Structure Interaction**, August 14-17, St. John's, Newfoundland, Canada (in press).
- Jordaan, I.J. and McKenna, R.F., 1988. "Modelling of Progressive Damage in Ice", **IAHR Symposium on Ice**, Sapporo, Japan, August, Proceedings Vol. II, pp. 585-624
- Jordaan, I.J. and Timco, G.W., 1988. "Dynamics of the Ice Crushing Process", **Journal of Glaciology**, Vol. 34, No. 118, pp. 318-326
- Jordaan, I.J., Maes, M. and Nadreau, J.P., 1988. "The Crushing and Clearing of Ice in Fast Spherical Indentation Tests", **OMAE '88**, Proceedings of the Seventh International Offshore Mechanics and Arctic Engineering Symposium, Vol. 4, New York, American Society of Mechanical Engineers, pp. 111-116

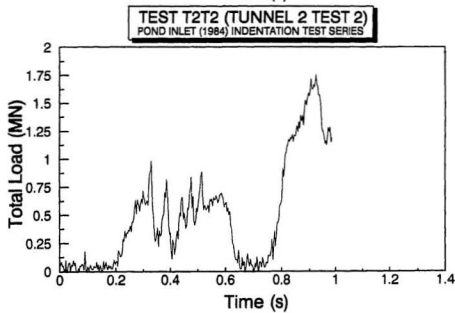
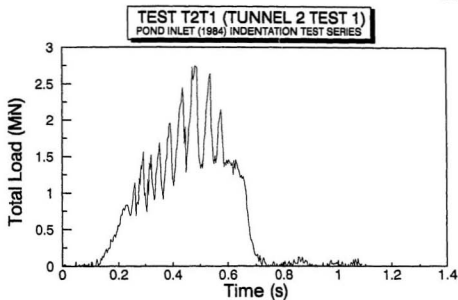
- Jordaan, I.J., McKenna, R.F., Duthinh, D., Fuglem, M., Kennedy, K., Maes, M.A. and Marshall, A., 1990. "Development of New Ice Load Models, prepared for Canada Oil and Gas Lands Administration (COGLA) by the Centre for Cold Ocean Resources Engineering (C-CORE), St. John's, NF, 167 pp.
- Kheisin, D.E. and Cherepanov, N.V., 1970. "Change of Ice Structure in the Zone of Impact of a Solid Body Against the Ice Cover Surface", *Problemy Arktiki Antarktiki*, Vol. 34, pp. 71-87. English translation in Israel Program for Scientific Translations, A.F. Treshnikov (ed.), Jerusalem, pp. 239-245
- Kry, P.R., 1978. **Continuous Crushing of Ice**, Esso Resources Canada Limited Report IPRT-28ME-78
- Kurdyumov, V.A. and Kheisin, D.E., 1976. "Hydrodynamic Model of the Impact of a Solid on Ice", translated from *Prikladnaya Mekhanika*, Vol. 12, No. 10, pp. 103-109
- Leonard, R.W., 1898. "Masonry Pier Moved by Ice and Replaced", *Transactions of the Canadian Society of Civil Engineers*, Vol. 12
- Määttänen, 1977. "Ice Force Measurements at the Gulf of Bothnia by the Instrumented Kemi I Lighthouse", **POAC '77**, Proceedings of the Fourth International Conference on Port and Ocean Engineering Under Arctic Conditions, St. John's, Newfoundland, Canada, 11 pp.
- Määttänen, 1975. "Experiences of Ice Forces Against a Steel Lighthouse Mounted on the Seabed, and Proposed Constructional Refinements", **POAC '75**, Proceedings of the Third International Conference on Port and Ocean Engineering Under Arctic Conditions, pp. 857-869.
- Metje, M. Danielwicz, B.W. and Hoare, R., 1981. "On Measuring Large Scale Ice Forces: Hans Island 1980", **POAC '81**, Proceedings of the Sixth International Conference on Port and Ocean Engineering Under Arctic Conditions. Quebec, Canada, Vol. II, pp. 629-642.
- Michel, 1978. **Ice Mechanics**, Les Presses de L'Université Laval, Quebec
- Nadreau, J.-P., 1987. "Ice-Induced Dynamic Behavior of Structures", **Oceans '87**, Halifax, Proceedings Vol. 1, pp. 30-34
- Nevel, Donald E., 1986. "Iceberg Impact Forces", **IAHR Symposium on Ice**, Proceedings Vol. III, Iowa City, pp. 345-369
- Peyton, H.R., 1966. "Sea Ice Forces", **Ice Pressures Against Structures**, Proceedings of a Conference held at Laval University, Quebec, November 10-11, National Research Council of Canada Technical Memorandum No. 92, pp., 117-123

- Peyton, H.R., 1968. "Ice and Marine Structures", **Ocean Industry**, March, pp. 40-44.
- Pilkington, R., Blanchet, D. and Metge, M., 1983. "Fullscale Measurements of Ice Forces on an Artificial Island", **POAC '83**, Seventh International Conference on Port and Ocean Engineering Under Arctic Conditions, Helsinki, Finland, Proceedings Vol. 4, pp. 818-834
- Riska, K., 1987. **On the Mechanics of the Ramming Interaction Between a Ship and a Massive Ice Floe**, Espoo 1987, Technical Research Centre of Finland (VTT) Publication 43, 86 pp.
- Sanden, E.J. and Neill, C.R., 1968. "Determination of Actual Forces on Bridge Piers Due to Moving Ice", Proceedings of the Convention of the **Canadian Good Roads Association**, pp. 405-420.
- Schlichting, H., 1968. **Boundary Layer Theory**, Translated by J. Kestin, McGraw-Hill Book Company, Inc., New York, 6th edition
- Spiegel, M.R., 1981. **Applied Differential Equations**, Prentice-Hall, Inc., Englewood Cliffs, New Jersey, 654 pp.
- Stone, B.M., Jordaan, I.J., Jones, S.J. and McKenna, R.F., 1989. "Damage of Isotropic Polycrystalline Ice Under Moderate Confining Pressures", **POAC '89**, Proceedings of the 10th International Conference on Port and Ocean Engineering Under Arctic Conditions, Lulea, Sweden
- Timco, G.W., 1986. "Indentation and Penetration of Edge-Loaded Freshwater Ice Sheets in the Brittle Range", **Fifth OMAE Symposium**, Proceedings Vol. IV, pp. 444-452
- Timco, G.W. and Jordaan, I.J., 1988. "Time-Series Variations in Ice Crushing", **POAC '87**, Proceedings of the 9th International Conference on Port and Ocean Engineering Under Arctic Conditions, Fairbanks, Alaska, pp.
- Tunik, A.L., 1989. "Ice Impact Pressure: More Questions Than Answers", **IUTAM/IAHR Symposium on Ice Structure Interaction**, August 14-17, St. John's, Newfoundland, Canada (in press)
- Xiao, J., 1990. Personal communication: elastic solution of deflection for the spherical indentation problem.

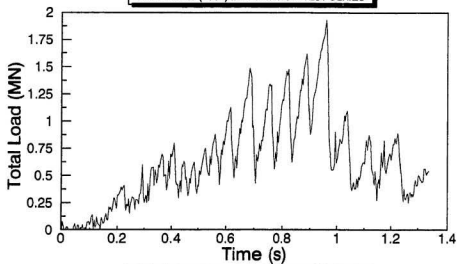
# **Appendix A**

## **Pond Inlet (1984) Data Summary**

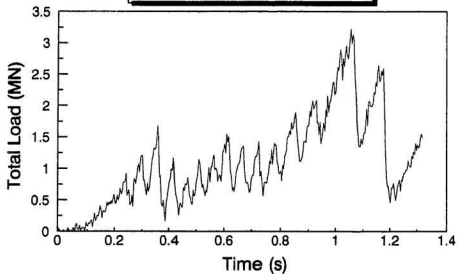
## 0.5 m<sup>2</sup> Load-Time Records



**TEST T3T3 (TUNNEL 3 TEST 3)**  
**POND INLET (1984) INDENTATION TEST SERIES**

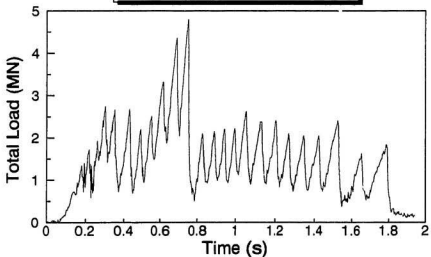


**TEST T3T4 (TUNNEL 3 TEST 4)**  
**POND INLET (1984) INDENTATION TEST SERIES**

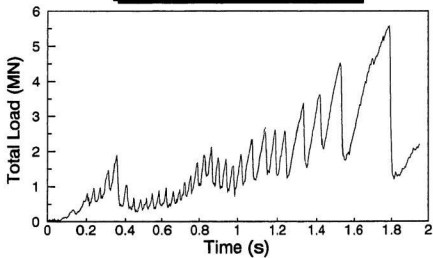


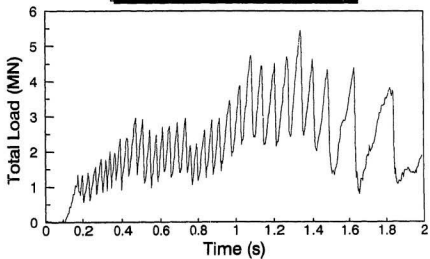
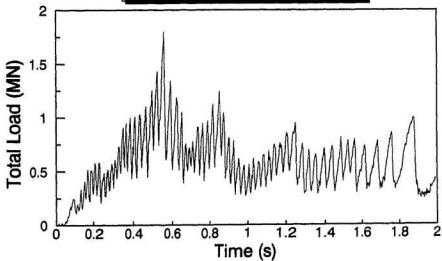
**1.0 m<sup>2</sup> Load-Time Records**

**TEST T1T4 (TUNNEL 1 TEST 4)**  
**POND INLET (1984) INDENTATION TEST SERIES**



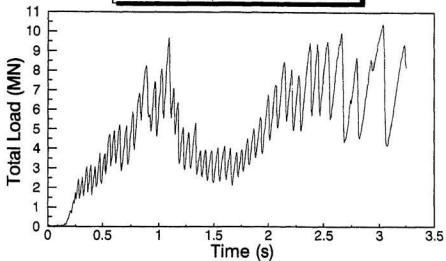
**TEST T2T5 (TUNNEL 2 TEST 5)**  
**POND INLET (1984) INDENTATION TEST SERIES**



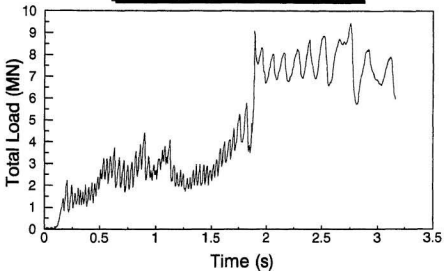
**TEST T2T6 (TUNNEL 2 TEST 6)**  
POND INLET (1984) INDENTATION TEST SERIES**TEST T4T1 (TUNNEL 4 TEST 1)**  
POND INLET (1984) INDENTATION TEST SERIES

### **3.0 m<sup>2</sup> Load-Time Records**

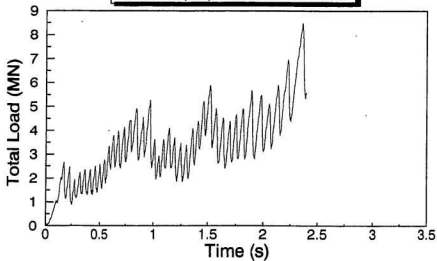
**TEST T1T5 (TUNNEL 1 TEST 5)**  
POND INLET (1984) INDENTATION TEST SERIES



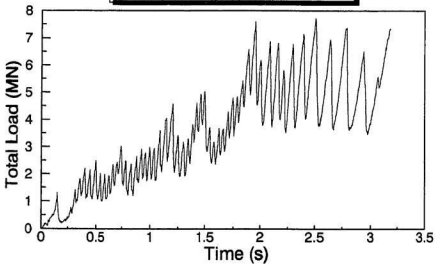
**TEST T3T2 (TUNNEL 3 TEST 2)**  
POND INLET (1984) INDENTATION TEST SERIES



**TEST T4T2 (TUNNEL 4 TEST 2)**  
POND INLET (1984) INDENTATION TEST SERIES



**TEST T4T3 (TUNNEL 4 TEST 3)**  
POND INLET (1984) INDENTATION TEST SERIES



## **Pond Inlet Pressure Cell Data**

Size (m <sup>2</sup> )	Test I.D.	Peak and Mean Pressures (MPa)									
		Cell 1		Cell 2		Cell 3		Cell 4		Cell 5	
		Peak	Mean	Peak	Mean	Peak	Mean	Peak	Mean	Peak	Mean
0.02	T1T1	35	13								
	T2T4	44	6								
	T3T5	50	26								
	T4T6	48	13								
0.10	T1T2	37	17								
	T1T3	56	27								
	T2T3	55	30								
	T4T4	56	25								
1.0	T1T4	31	6								
	T2T5	42	9								
	T4T1	25	4								
	T2T6	48	15								
0.5	T2T1	58	19	37	17	0	0	10	6		
	T2T2	54	11	5	1	0	0	0	0		
	T3T3	56	10	40	10	0	0	8	1		
	T3T4										
3.0	T1T5	60	10	12	5	9	4	3	2	10	2
	T3T2	-	-	18	5	9	1	3	1	49	20
	T4T2	-	-	11	3	7	1	0	0	0	0
	T4T3	-	-	51	10	12	4	0	0	4	1

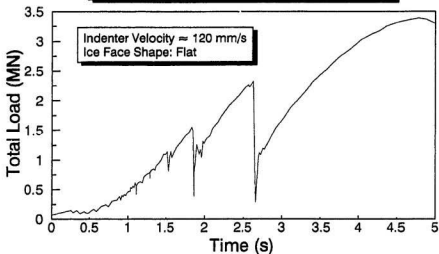
Table A.1: Pond Inlet Pressure Cell Data.

# Appendix B

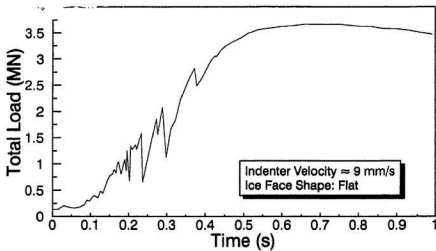
## Ice Island (1989) Data Summary

**TEST NRC03 (SPHERICAL INDENTER)**

ICE ISLAND (1989) INDENTATION TEST SERIES

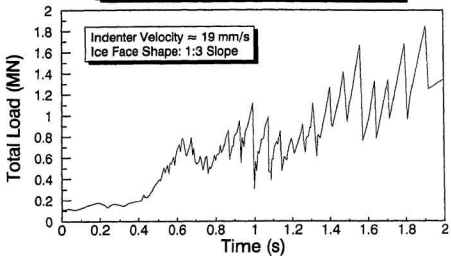
**TEST NRC05 (SPHERICAL INDENTER)**

ICE ISLAND (1989) INDENTATION TEST SERIES

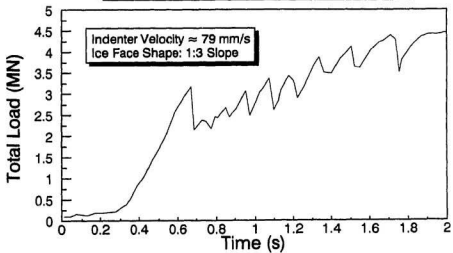


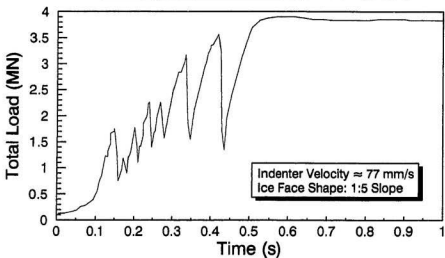
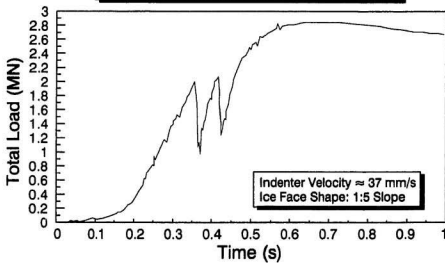
**TEST NRC06 (FLEXIBLE INDENTER)**

ICE ISLAND (1989) INDENTATION TEST SERIES

**TEST NRC06 (FLEXIBLE INDENTER)**

ICE ISLAND (1989) INDENTATION TEST SERIES



**TEST NRC08 (MEGANEWT INDENTER)**  
ICE ISLAND (1989) INDENTATION TEST SERIES**TEST NRC10 (MEGANEWT INDENTER)**  
ICE ISLAND (1989) INDENTATION TEST SERIES

## Appendix C

Approximation for Small  $\theta_t$

Developed in Section 5.1, the total load on a spherical indenter was given by

$$F = \frac{2\pi\nu_o\mu R^4}{\ell^3} (2 - 3\cos\theta_t + \cos^3\theta_t). \quad (\text{C.1})$$

For the case of an indenter with large radius of curvature,  $R$ , and correspondingly small indentation angle,  $\theta_t$ , further simplification of Equation C.1 is possible using the power series expansion for  $\cos\theta_t$ , i.e.,

$$\cos x = 1 - \frac{x^2}{2!} + \frac{x^4}{4!} - \dots, -\infty < x < \infty. \quad (\text{C.2})$$

Similarly,

$$\cos^3 x = \left(1 - \frac{x^2}{2!} + \frac{x^4}{4!}\right)^3. \quad (\text{C.3})$$

Letting  $y = -x^2/(2!) + x^4/(4!)$ , then

$$\cos^3 x = (1 + y)^3 \quad (\text{C.4})$$

$$\cos^3 x = 1 + 3y + 3y^2 + y^3. \quad (\text{C.5})$$

For small  $x$ , the  $y^3$  term will be negligible, leaving

$$\cos^3 x = 1 + 3\left(-\frac{x^2}{2!} + \frac{x^4}{4!}\right) + 3\left(-\frac{x^2}{2!} + \frac{x^4}{4!}\right)^2 \quad (\text{C.6})$$

$$\cos^3 x = 1 - 3\frac{x^2}{2!} + 3\frac{x^4}{4!} + 3\left(\frac{x^4}{2!^2} - \frac{x^6}{4!} + \frac{x^8}{4!^2}\right). \quad (\text{C.7})$$

The second and third terms of the bracketed expression above are negligible as well, leaving

$$\cos^3 x = 1 - 3\frac{x^2}{2!} + 3\frac{x^4}{4!} + 3\frac{x^4}{2!^2}. \quad (\text{C.8})$$

The term  $(2 - 3\cos\theta_t + \cos^3\theta_t)$  from Equation C.1 may be computed by summing the terms from the series expansion as follows:

$$\begin{array}{r|rrrr} 2 & 2 & & & \\ 3\cos\theta_t & -3 & +3\theta_t^2/2 & -3\theta_t^4/24 & \\ \cos^3\theta_t & 1 & -3\theta_t^2/2 & +3\theta_t^4/24 & +3\theta_t^4/4 \\ \hline & 0 & 0 & 0 & 3\theta_t^4/4 \end{array}$$

Total load on the indenter for the case of large  $R$  and small  $\theta_t$  may therefore be expressed as:

$$F = \frac{2\pi\nu_o\mu R^4}{\ell^3} (3\theta_t^4/4) \quad (\text{C.9})$$

$$F = \frac{3\pi\nu_o\mu R^4 \theta_t^4}{2\ell^3}. \quad (\text{C.10})$$







